ESAT-6 undergoes self-association at phagosomal pH and an ESAT-6 specific nanobody restricts M. tuberculosis growth in macrophages

Timothy A Bates[1], Mila Trank-Greene[1], Xammy Nguyenla[1], Aidan Anastas[1], Sintayehu K Gurmessa[1], Ilaria R Merutka[1], Shandee D Dixon[1], Anthony Shumate[2], Abigail R Groncki[1], Matthew AH Parson[3], Jessica R Ingram[4,†], Eric Barklis[1], John E Burke[3,5], Ujwal Shinde[2], Hidde L Ploegh[4], Fikadu G Tafesse[1,6]

[1]Department of Molecular Microbiology and Immunology, Oregon Health & Sciences University, Portland, Oregon, United States.

[2]Department of Chemical Physiology and Biochemistry, Oregon Health & Science University, Portland, Oregon, United States.

[3]Department of Biochemistry and Microbiology, University of Victoria, Victoria, Canada.

[4]Program in Cellular and Molecular Medicine, Boston Children's Hospital, Harvard Medical School, Boston, Massachusetts, United States.

[5]Department of Biochemistry and Molecular Biology, The University of British Columbia, Vancouver, Canada.

[†]Deceased April 18, 2018

[6]Correspondence to tafesse@ohsu.edu

Abstract

Mycobacterium tuberculosis (Mtb) is known to survive within macrophages by compromising the integrity of the phagosomal compartment in which it resides. This activity

primarily relies on the ESX-1 secretion system, predominantly involving the protein duo ESAT-6 and CFP-10. CFP-10 likely acts as a chaperone, while ESAT-6 likely disrupts phagosomal membrane stability via a largely unknown mechanism. we employ a series of biochemical analyses, protein modeling techniques, and a novel ESAT-6-specific nanobody to gain insight into the ESAT-6's mode of action. First, we measure the binding kinetics of the tight 1:1 complex formed by ESAT-6 and CFP-10 at neutral pH. Subsequently, we demonstrate a rapid self-association of ESAT-6 into large complexes under acidic conditions, leading to the identification of a stable tetrameric ESAT-6 species. Using molecular dynamics simulations, we pinpoint the most probable interaction interface. Furthermore, we show that cytoplasmic expression of an anti-ESAT-6 nanobody blocks Mtb replication, thereby underlining the pivotal role of ESAT-6 in intracellular survival. Together, these data suggest that ESAT-6 acts by a pH dependent mechanism to establish two-way communication between the cytoplasm and the Mtb-containing phagosome.

Introduction

Tuberculosis (TB), caused by *Mycobacterium tuberculosis* (Mtb), is a major global health concern, claiming over 1.6 million lives annually. Mtb is highly adept at evading the immune system, and it can persist within an infected person for decades. This situation is worsened by the nearly 1.7 billion people globally who harbor a dormant Mtb infection (Houben and Dodd, 2016), coupled with the rising trend of drug-resistant TB cases (World Health Organization, 2022).

To successfully establish an infection in the host, Mtb utilizes a plethora of virulence factors delivered via its several ESX-secretion systems. Studies have indicated that Mtb has the ability to damage the phagosomal membrane, a process that is heavily reliant on the activity of the ESX-1 secretion system (Conrad et al., 2017; López-Jiménez et al., 2018; Schnettger et al.,

2017). Currently, the most probable candidate driving ESX-1 dependent lytic activity is the well-known T cell antigen, the 6 kDa early secreted antigenic target (ESAT-6, or EsxA)) (Andersen et al., 1995; Sørensen et al., 1995), after which the ESX family of T7SSs was originally named (Gey van Pittius et al., 2001). Secretion of the various ESX-1 substrates are known to be highly complex and interdependent, and while the full scope of ESX-1 components and substrates is still being worked out, many individual ESX-1 component knockouts are known to phenocopy the ESAT-6 deletion, indicating that ESAT-6 itself is responsible for the lion's share of the activity (Chen et al., 2012; Clemmensen et al., 2017; Cronin et al., 2022; Lienard et al., 2020; Sanchez et al., 2020).

Over the last few decades, there have been numerous studies focused on uncovering the possible mechanism of membrane lysis by ESAT-6 (Augenstreich et al., 2020; Conrad et al., 2017; de Jonge et al., 2007; Kinhikar et al., 2010; Koo et al., 2008; Lienard et al., 2020; Osman et al., 2022), and how this might lead to escape of Mtb from the phagosome (Houben et al., 2012). However, the field has been plagued by setbacks such as the discovery that many studies prior to 2017 showing membrane disruption by ESAT-6 were confounded by the contamination with the detergent ASB-14, which was originally added to remove endotoxin (Conrad et al., 2017). Consequently, most recent studies have focused on the use of intact bacteria in assays, frequently with the closely related *Mycobacterium marinum* (Mm), to avoid using recombinant proteins. The conclusions of these experiments are complicated by the interdependent nature of ESX-1 structural components, chaperones, and substrates (Augenstreich et al., 2020; Osman et al., 2022; Santucci et al., 2022). Mm has been a valuable model for working out ESX-1 and ESAT-6 function, and many of the key studies in the field have used Mm exclusively. However, the unique characteristics of Mm compared to Mtb can sometimes leads to differing results, and conclusions drawn from one species do not always apply to the other (Bosserman et al., 2019; Carlsson et al., 2009; Lienard et al., 2020; Osman et

al., 2022; Smith et al., 2008). This is important because the membranolytic activity of the ESX-1 seems to be highly context dependent, and more biochemical work is needed to work out the specific contributions of ESAT-6 to the membrane disruption phenotype.

Despite extensive research, the precise mechanism of ESAT-6 action remains elusive. This study aims to bridge this gap by performing comprehensive biochemical and cellular investigations of ESAT-6 under neutral and acidic conditions. We use biolayer interferometry (BLI) to measure the tight association between ESAT-6 and CFP-10, and the pH dependent ESAT-6 self-association. We use fluorescence microscopy to directly observe formation of large ESAT-6 complexes, and we measure the stoichiometry of ESAT-6 under different pH conditions using multi-angle light scattering. We then use molecular dynamics-based modeling to evaluate the most likely modes of ESAT-6 interaction. We also generated a novel ESAT-6-binding alpaca-derived nanobody, E11rv, to further define the significance of ESAT-6 during Mtb infection. We perform biochemical characterization of E11rv, as well as functional testing, which showed inhibition of Mtb growth inside macrophages treated with E11rv or expressing cytoplasmic E11rv.

Results

Recombinant ESAT-6 and CFP-10 purification

In seeking to perform functional studies of ESAT-6 and CFP-10, we produced recombinant protein using *E. coli* expression plasmids available from BEI Resources: pMRLB.7 (NR-50170) containing ESAT-6, and pMRLB.46 (NR-13297) containing CFP-10. Both of these plasmids have been used extensively in literature, including many of the most influential biochemical characterization studies (Augenstreich et al., 2020; Behura et al., 2019; Chen et al., 2019; Choi et al., 2010; Conrad et al., 2017; de Jonge et al., 2007; Eitson et al., 2012; Gallegos et al., 2008; Harrison et al., 2014; Koyuncu et al., 2021; Lim et al., 2016; Mukherjee et al., 2007;

Niazi et al., 2015; Osman et al., 2022; Pathak et al., 2007; Peng et al., 2011; Refai et al., 2015; Smith et al., 2008; Stavri et al., 2012; Vesosky et al., 2010; Woolhiser et al., 2007; Xiao et al., 2016; Yang et al., 2008). The specification sheet for pMRLB.7 indicates that it includes a C-terminal FALE solubility tag and subsequent Histidine affinity tag while pMRLB.46 indicates that it contains only a C-terminal Histidine tag. We performed sequencing of both plasmids (Figure 1A), and noticed a stretch of 10 additional amino acids ahead of the reported tags in the pMRLB.7 plasmid (Figure 1–figure supplement 1). The precise amino acid sequence of the pMRLB.46 plasmid has not been reported, but it appears to contain 4 additional amino acids ahead of the expected tag. Importantly, we were able to confirm that the full and complete sequences of ESAT-6 and CFP-10 are each contained in their respective plasmids, and the inconsistencies fall within the C-terminal tag regions of each protein (Figure 1A).

Expression and purification by Nickel-NTA chromatography resulted in bands of the expected sizes by SDS-PAGE and His_6-specific western blot (Figure 1B). Amino acid sequences of the recombinant proteins were also confirmed by mass spectrometry (MS), where it was observed that CFP-10 undergoes N-terminal methionine excision in our *E. coli* expression system (Figure 1–figure supplement 2) (Giglione et al., 2004; Hirel et al., 1989). Size exclusion chromatography (SEC) showed appropriate relative retention volumes and combining equimolar quantities of ESAT-6 with CFP-10 resulted in a leftward shift, suggesting correct dimerization (Figure 1C).

Dimerization of ESAT-6 and CFP-10 at neutral pH

To validate that ESAT-6 and CFP-10 are forming a native dimer, we next performed native-PAGE with different ratios of the two proteins (Figure 2A). We incubated ESAT-6 and CFP-10 for 1 hour at 4°C prior to running the gels, combining them in different ratios. The isoelectric point of ESAT-6 and CFP-10 are both quite low, for our constructs they are 5.18 (net charge -8.22 at pH 7.4) and 5.72 (net charge -5.27 at pH 7.4), respectively. Thus, we oriented

the positive electrode toward the bottom of the gel. As expected, we observed that ESAT-6 ran faster than CFP-10. Combinations of each showed a distinct third band of intermediate charge which was greatest in the 1:1 mixture and absent in each pure protein, indicating formation of a 1:1 complex with no intermediate species. This aligns with our results from Fig 1C, and aligns with historical research on the interaction between ESAT-6 and CFP-10 (Poulsen et al., 2014; Renshaw et al., 2005, 2002).

Another commonly used test of ESAT-6 function is hemolysis, or the ability to damage red blood cell (RBC) membranes and release hemoglobin. Historical studies reported that ESAT-6 was able to cause hemolysis, but Conrad et al. discovered that most of this hemolytic activity was due to detergent contamination with ASB-14, which is commonly added during the wash steps of Nickel-NTA purification to remove endotoxin (Conrad et al., 2017). Our recombinant ESAT-6 was produced without detergent, and we confirmed that it was not able to induce hemolysis at any pH between 4.5 and 7.5 (Figure 2–figure supplement 1). However, the hemolysis assay still finds contemporary use when testing the ability of whole bacteria to induce membrane damage in an ESX-1 and contact-dependent manner (Augenstreich et al., 2020; Bosserman et al., 2019; Conrad et al., 2017; Osman et al., 2022). In such experiments, RBCs are mixed with log-phase bacterial cultures at high MOI and pelleted by centrifugation to force direct contact. Similar to previous reports, we found that *Mycobacterium marinum* (Mm) is capable of efficiently causing hemolysis within 2 hours (Figure 2B). In contrast, we found that Mtb was incapable of hemolysis over a similar time frame. It is well established that Mm-induced hemolysis is ESX-1 dependent, but our results suggest that there are some differences in Mtb that affect the rate or extent of hemolysis. One previous study was able to induce hemolysis using Mtb, but this required 48 hours instead of the typical 2 (Augenstreich et al., 2020).

Binding kinetics of ESAT-6 and CFP-10

To measure the binding strength of ESAT-6 and CFP-10 we developed a biolayer interferometry (BLI) assay to measure their interactions (Figure 3A). We first measured the ability of ESAT-6 and CFP-10 to form homo-oligomers or hetero-oligomers (Figure 3B), and found that they preferentially formed hetero-oligomers. ESAT-6 showed a small, but measurable amount of self-association, while CFP-10 showed no self-association. The dissociation constant (K_D) of the ESAT-6/CFP-10 heterodimer has not hitherto been directly measured, but Renshaw et al. estimated an upper bound of 10nM (Renshaw et al., 2002). We performed a detailed measurement of the ESAT-6/CFP-10 association and measured a K_D of 220 pM, indicating exceptionally tight binding (Figure 3C). ESAT-6 self-association resulted in reduced overall binding to the sensor and displayed a rapid on rate, but also a rapid off rate (Figure 3D). The curve shape is suggestive of something other than traditional 1:1 binding, but for comparison purposes we calculated an apparent K_D of approximately 1.5 μM, weaker than that of the ESAT-6/CFP-10 association.

The pH of the Mtb-containing compartment typically ranges from 4.5 in IFN-γ activated macrophages to 6.2 in non-activated macrophages (MacMicking et al., 2003; Vandal et al., 2008). Because Mtb can exists in an acidified compartment, we tested whether ESAT-6 binding changes under low pH conditions. Surprisingly, ESAT-6 displayed robust self-association at pH 4.5 (Figure 3E), resulting in several-fold more mass attaching to the sensor than even the ESAT-6/CFP-10 association at neutral pH. The apparent K_D for this interaction was slightly weaker than ESAT-6 self-association at neutral pH, but the total amount of binding was 20-30-fold greater, suggesting that low pH conditions trigger ESAT-6 to assemble into larger complexes. Further, there have been conflicting reports on whether ESAT-6 and CFP-10 dissociate from each other at low pH (de Jonge et al., 2007; De Leon et al., 2012; Lightbody et al., 2008). Our results support the stable interaction of ESAT-6 and CFP-10 at low-pH (Figure

3F), which exhibits an extremely tight apparent K_D of 0.4 pM at pH 4.5: however, this is likely due to the multivalent ESAT-6 self-association occurring in this condition (Figure 3G). To determine the precise pH at which ESAT-6 self-association becomes dominant, we performed BLI experiments at half pH units from 4.5 to 6.5 (Figure 3H). We found that 5.0 was the most basic pH at which increased self-association occurred.

Formation of large ESAT-6 complexes at pH 4.5

The response from pH 4.5 ESAT-6 biosensors appeared to increase past the typical association time of our BLI assay. Because of this, we extended the binding time to 20 minutes (Figure 4A), but the increasing self-association of ESAT-6 continued at roughly the same rate throughout. To explore the possibility of complex formation and to determine the timeframe over which this occurs, we next performed turbidity assays in which 50 µM of either ESAT-6 or CFP-10 were brought to pH 4.5 or 7.5 and A_{350} was measured by plate reader for 1 hour (Figure 4B). We observed an increase in turbidity at pH 4.5 but not 7.5 which was greater for ESAT-6 than CFP-10, in line with previous findings (De Leon et al., 2012).

The BLI experiments we have shown thus far using the streptavidin-coated biosensors (Figure 3A), have utilized ESAT-6 which had been biotinylated using succinimide chemistry (ChromaLINK, Vector labs) allowing for precise quantification of incorporated biotin. Using 3 molar equivalents of labeling reagent, we obtained ESAT-6 with an average of 0.99 biotins/protein. However, succinimide chemistry can label any primary amine including the N-terminus and lysine residues. ESAT-6 normally contains 3 lysines, and the pMRLB.7 construct contains 1 additional lysine for a total of 4 (Figure 4C). Because it is unknown which region of the protein may be involved in self-association, we generated an additional ESAT-6 construct capable of C-terminal site-directed biotinylation via sortase-mediated transpeptidation via an LPETG motif (Figure 4C) (Guimaraes et al., 2013; Popp et al., 2009). We performed additional

BLI experiments using the ESAT-6-LPETG construct and were able to verify similar behavior at neutral and acidic pH (Figure 4D-F).

Stoichiometry of ESAT-6 complexes

We next visualized the large ESAT-6 complexes by fluorescence microscopy in order to get an idea of their scale. We mixed unmodified ESAT-6 with ESAT-6-LPETG-Biotin at a 10:1 ratio and incubated on a poly-lysine coated coverslip, fixed, then stained with streptavidin-AF488 to visualize ESAT-6 complexes. Fluorescence microscopy shows the development of individual strands with the appearance of a heavily kinked thread or beads on a string (Figure 5A). These structures were not present at neutral pH or when 6M guanidine was added to acidified ESAT-6.

To analyze the stoichiometry of these complexes, we next performed SEC coupled with multi-angle light scattering (MALS), which can measure the molecular weight of complexes as they elute from the SEC column. At pH 7.5, we observed a single peak with an approximate molecular weight of 21 kDa, which most likely corresponds to an ESAT-6 homodimer (Figure 5B). We did not observe the presence of any monomeric ESAT-6, indicating that it likely self-pairs in the absence of CFP-10. This agrees with our BLI results from (Figure 3C). At pH 4.5, we were surprised to see a single, well-defined peak at 46 kDa, most likely corresponding to a tetramer (Figure 5C). No measurable monomer, dimer, or higher molecular weight complexes were observed. While it is not surprising that the high molecular weight complexes observed (Figure 5A) were unable to traverse the SEC column intact, it was unexpected that tetramers would be the only species observed.

To address the question of the likely conformation of the homodimer and tetramer, we performed modeling experiments using docking followed by molecular dynamics (MD) simulations to estimate the most stable conformations. We started with a homology model

based on previously reported structures of the ESAT-6/CFP-10 heterodimer (PDB: 3FAV, 4J11, 4J7K, 4J10 and 4J7J) (Fan et al., 2015; Poulsen et al., 2014). To estimate the structure of the ESAT-6 monomer, we then performed a molecular dynamics simulation to observe the structural stability of the protein's conformation. We observed that the energy-minimized structure of monomeric ESAT-6 strongly resembles its conformation in the heterodimer. The helix-turn-helix structure exhibits strong amphipathic nature, with both helices aligning to form a hydrophobic face flanked by charged residues (Figure 5D).

We next modeled an ESAT-6 homodimer, starting again with a homology model based on the heterodimer followed by a molecular dynamics simulation. The homodimer model showed head-to-tail alignment of the ESAT-6 monomers associating via their hydrophobic faces and stabilized on either side by salt bridges (Figure 5E). This homodimer model represents a likely conformation of the species observed in the pH 7.5 SEC-MALS experiment (Figure 5B).

To model the tetrameric species observed in the acidic SEC-MALS experiment (Figure 5C), we performed docking of ESAT-6 homodimers and then a molecular dynamics simulation of the lowest energy conformation observed in docking. We observed the dimers interacting in a head-to-tail orientation via their hydrophilic faces, supported by salt bridges (Figure 5F). In the tetramer model, some of the charged residues, such as Lys_{67}, which had previously supported the dimer interface, switched orientations to support the tetramer interface.

For each of these models, the molecular dynamics informs us about the proteins' conformational stability. The root mean square fluctuation (RMSF) quantifies the amount of movement along the peptide backbone for each residue, with lower values equating to more stability. We performed molecular dynamics experiments for ESAT-6 in monomer, dimer, and tetramer forms in order to evaluate the stability of each species (Figure 5G). In general, the α-helices of ESAT-6 are stable, while the C- and N-termini are highly flexible. However, in the monomeric form, the residues between 20 and 50 exhibit increased flexibility at pH 7.5. At pH

4.5, the monomeric form exhibits increased flexibility along a majority of the backbone. At both pH values, dimerization (and tetramerization) result in greater overall stability. At pH 7.5, the average RMSF of the monomer is 2.51, which reduces to 2.33 for the dimer due to the reduced flexibility between residues 20 and 50. The tetramer is only marginally more stable, at 2.27. At pH 4.5, the difference between each state is even more pronounced, with an RMSF of 2.74, 2.04, and 1.94 for the monomer, dimer, and tetramer, respectively.

Generation and characterization of an ESAT-6 specific nanobody

We generated an ESAT-6-specific alpaca-derived nanobody using our previously reported phage display method (Alfadhli et al., 2021; Bachran et al., 2017; Weinstein et al., 2022). E11rv was generated by immunization and panning against pMRLB.7 ESAT-6. Following initial isolation, we performed biochemical characterization, starting with ELISA experiments to determine the EC_{50} of E11rv, which was found to be 1.26 µM (Figure 6A). We then determined the binding kinetics via BLI, which we performed on both pMRLB.7 ESAT6 as well as our ESAT-6-LPETG construct to ensure that the tag was not essential for binding (Figure 6B-C). E11rv bound similarly to ESAT-6 and ESAT-6-LPETG with K_Ds of 331 nM and 376 nM, respectively.

To determine the binding site, we performed hydrogen deuterium exchange experiments with ESAT-6 (Harris et al., 2023; Masson et al., 2019; Rathinaswamy et al., 2021). This involves incubating either apo or E11rv-bound ESAT-6 in D_2O buffer for different lengths of time. The deuterium will exchange with acidic protons in the protein at different rates depending on the solvent exposure, giving insights into which areas of the protein are more tightly folded, or shielded by protein-protein interactions with a nanobody (Figure 6D-F). Digestion followed by MS allows quantification of the extent of deuteration along the peptide backbone and concomitant binding site estimation. For E11rv, we observed decreased deuteration compared to apo around positions 50-65 (on the C-terminal helix, near the loop), and to a lesser extent positions 98-110 (within the tag). The region between these segments, from residues 66-94,

displayed an increase in solvent exposure, as did residues 14-28, on the opposing helix directly across from 66-94. A likely explanation for this pattern is that E11rv binds around residues 50-65, and that this somehow destabilizes the C-terminal portion of the helix or separates the helices enough to allow more solvent exposure between helices. It is unclear how the small region within the tag might be involved, but Fig 6B suggests that the positioning of the tag has little impact on binding, and this region is predicted to be largely unstructured.

E11rv inhibits Mtb replication in macrophages.

We next performed functional testing of E11rv using two complementary approaches for measuring the growth and viability of internalized Mtb in macrophages. The first of these experiments used a live/dead reporter strain of Mtb based on H37Rv which constitutively expresses mCherry and dox inducible expression of GFP, which has been shown to correlate with CFU count (Martin et al., 2012). We infected THP-1 cells with live/dead reporter Mtb pre-incubated with E11rv or an isotype control, then allowed the infection to proceed for 3 days before inducing GFP with doxycycline for 24 hours. After fixing and staining for actin to reveal the location of cells, we performed fluorescence microscopy on the infected cells. We then used CellProfiler to identify all Mtb within images by their red fluorescence and calculated the GFP/RFP ratio for each identified bacterium (Stirling et al., 2021). In this experiment, we found that E11rv led to a statistically significant reduction in Mtb viability (Figure 7A,B).

The second functional assay we performed was based on continuous growth measurement of luminescent LuxABCDE-expressing Mtb (Andreu et al., 2010; Leddy et al., 2023). We prepared stable THP-1 cell lines with cytoplasmic expression of E11rv or an isotype nanobody. We then infected the nanobody-expressing THP-1 cells with luminescent Mtb and monitored their growth continuously via plate reader for 5 days, and we found that E11rv reduced the growth rate substantially (Figure 7C). Over the full 5 days, the isotype-expressing

cells allowed the Mtb to grow to 6-fold over its starting value while the E11rv-expressing cells reduced this to just under 3-fold.

Discussion

This study has several key findings. Firstly, ESAT-6 undergoes rapid self-association into large complexes at pH levels below 5.0, and this may be preceded by formation of stable tetramers. Second, in the absence of CFP-10, ESAT-6 exists as a homodimer at neutral pH. Third, our nanobody, E11rv, binds to ESAT-6 and can inhibit the growth of Mtb inside cells when treated externally or via cytoplasmic expression.

The issue of incomplete information about the amino acid sequence of one of the most widely used ESAT-6 constructs is surprising, but none of the data we have generated suggested a practical difference with differently tagged constructs. Previous studies have found major differences in function between recombinant ESAT-6 in general when compared with "native" ESAT-6 purified from Mtb cultures, which are typically purified using much harsher techniques than recombinant protein due to the lack of affinity tags. One attractive theory for the observed difference between recombinant and native ESAT-6 which is gaining traction is N-terminal acetylation being required for ESAT-6 function, but this has not yet been proven in Mtb infection (Aguilera et al., 2020; Collars et al., 2023; Mba Medie et al., 2014; Okkels et al., 2004). The most commonly given reason for the importance of N-acetylation is that acetylated ESAT-6 is more easily released from CFP-10 under acidic conditions. Our results suggest that purified ESAT-6 exists in a dimerized state in the absence of CFP-10, but our Native-PAGE (Figure 2A) and SEC (Figure 1C) demonstrate that purified ESAT-6 has no trouble interacting with CFP-10 to form a 1:1 complex. It is unclear whether the observed 1:1 complex is an ESAT-6/CFP-10 heterodimer formed by exchange between ESAT-6 and CFP-10 homodimers, or if we are instead observing formation of a tetramer composed of one each ESAT-6 and CFP-10

homodimers. Further, our low pH BLI results (Figure 3F) suggest that self-associated ESAT-6 has no difficulty interacting with CFP-10.

Our modeling and SEC-MALS data suggest that ESAT-6 can interact with itself using both of its faces, one of which is hydrophobic, and one of which is hydrophilic; and both of which are supported by salt bridges formed by charged residues at either edge. This implies that ESAT-6 may still be able to self-associate within membranes via its hydrophilic face. This agrees with the putative requirement for compartment acidification in order to drive membrane damage, as our data suggests that low pH is required for self-association at this interface, but likely does not affect the hydrophobic interface, which must then require a different mechanism for dissociation and membrane insertion. Some have suggested that other mycobacterial factors may help facilitate the membrane insertion of ESAT-6, such as phthiocerol dimycocerosates (Augenstreich et al., 2020, 2017).

Modeling approaches have also been used previously to propose an organized ESAT-6 pore structure using similar logic, but these have yet to be supported by physical evidence (Karki et al., 2020; Refai et al., 2015). However, there is precedent for ESAT-6-like WXG proteins to form organized membrane channels, with a recent study demonstrating a pentameric EsxE/EsxF structure capable of membrane insertion and toxin trafficking (Tak et al., 2021). Critically, EsxE does not dissociate from EsxF in order to insert into the membrane. Such structures have yet to be observed with ESAT-6/CFP-10, but this may just be a matter of finding the appropriate conditions and reagents.

Finding molecular tools to interrogate the function of Mtb virulence factors remains a challenge due to the complexity of accessing Mtb in its native environment within the phagosome. The nanobody described here presents a novel way of targeting the bacteria *in situ*, which we demonstrated by modulating its growth using intracellularly expressed E11rv. Because E11rv showed functional effects both when added in the media and when expressed

inside the cell cytoplasm, it suggests a significant amount of communication between Mtb inside the phagosome and other compartments of the cell. This is consistent with the findings of many other studies which show numerous putative activities for ESAT-6 such as induction of apoptosis (Behura et al., 2019; Choi et al., 2010; Lim et al., 2016; Yang et al., 2015), inhibition of interferon-γ production (Kumar et al., 2012; Peng et al., 2011), inhibition of autophagy (Dong et al., 2016; Romagnoli et al., 2012; Yabaji et al., 2020), inhibition of antigen presentation (Sreejit et al., 2014), induction of type I interferon (Jang et al., 2018; Lienard et al., 2020), and a more recent study showing an ESX-1-dependent mechanism for incorporation of Mtb antigens into MHC-I presentation via cytosolic antigen processing (Leddy et al., 2023). Most of these functions rely on ESAT-6 getting into the cytoplasm, and this may occur via disruptions in the phagosomal membrane to establish two-way communication between compartments, or by complete phagosomal escape of Mtb into the cytoplasm and subsequent secretion of ESAT-6 directly into the cytoplasm.

Data availability

Source data for this manuscript can be found at DOI: 10.5281/zenodo.10798945.

Materials availability

Materials will be made available upon reasonable request to the corresponding author.

Acknowledgements

Competing interests

HLP serves as an advisor to and owns stock in Cerberus Therapeutics. HLP serves as a consultant to Johnson and Johnson, Immatics Therapeutics, Cue Biopharma, Revela Therapeutics, and Tiba Bio. JEB reports personal fees from Scorpion Therapeutics, Reactive therapeutics and Olema Oncology; and research grants from Novartis. All other authors declare that they have no competing interests.

Methods

Plasmids and primers

Plasmids

Name	Description	Source
pMRLB.7	ESAT-6 expression vector	BEI Resources, NR-50170
pMRLB.46	CFP-10 expression vector	BEI Resources, NR-13297
pMRLB.7-LPETG	ESAT-6-LPETG expression vector	This study
pHEN	Nanobody expression vector	(Hoogenboom et al., 1991)
pInducer20	Lentiviral expression vector	(Meerbrey et al., 2011)

Primers

Name	Sequence
T7 (sequencing primer)	TAATACGACTCACTATAGGG
ESAT-6-Fw	CCGGAAACCGGCGGCATCAAGCTTATCGATACCGTCGACCTC
ESAT-6-Rv	GCCGCCGGTTTCCGGGAGCTCTGCGAACATCCCAGTG

Cloning ESAT-6-LPETG

ESAT-6-LPETG was generated by in vivo assembly (IVA) as described previously (García-Nafría et al., 2016). PCR was performed on pMRLB.7 using ESAT-6-Fw and ESAT-6-Rv

primers using Q5 polymerase with the following recipe and cycle design. Reactions were treated with DpnI for 15 minutes at 37°C. 2 µL of reaction mixture was added directly to 50 µL of chemically competent DH5-α cells, incubated on ice for 30 minutes, heat shocked at 42 for 30 seconds, then immediately added to 200 µL of SOC, after which it was recovered for 30 minutes at 37°C and plated on Luria Bertani (LB)-ampicillin (amp) agar plates, and incubated overnight at 37°C. Clones were sequence confirmed before further use.

Expression and purification of ESAT-6 and CFP-10

pMRLB.7, pMRLB.46, and pMRLB.7-LPETG were transformed into *Escherichia coli* BL21 Rosetta rare codon competent cells. 25 mL Luria Bertani (LB) starter cultures were grown overnight at 37°C with shaking with 100 ug/mL ampicillin to stationary phase. Each starter culture was used to inoculate 1L of LB, which was then grown at 37°C until reaching an OD_{600} of 0.8, at which point it was induced with 0.1 mM IPTG for 4 hours at 37°C. Bacteria was pelleted by centrifugation at 6,000×g for 10 minutes, then frozen at –80°C. Pellets were thawed and resuspended in 25 mL of 10 mM Tris HCl, 300 mM NaCl, 10% glycerol, 10 mM Imidazole, 1 ug/mL DNase and RNase, 0.5 mg/ml Lysozyme, 10 mM DTT, and 1 tablet/100 mL Sigma fast EDTA free protease inhibitor (Lysis buffer) for 20 minutes. Lysates were sonicated on ice for 30 seconds on and 30 seconds off for a total of 5 minutes. Crude lysates were then clarified by centrifugated at 20,000×g for 20 minutes. Supernatant was decanted and spun again similarly. Ni-NTA beads were washed with 10 mM Tris HCl, 300 mM NaCl, 10 % glycerol (wash buffer). Lysate was applied to 0.5 mL of Ni-NTA beads per liter of bacteria and rocked for 1 hour at 4°C then poured over a 25 mL chromatography column. The column was then washed with 10 column volumes of wash buffer plus 10 mM Imidazole, and then eluted in 10 mL wash buffer plus 250 mM Imidazole. Protein containing fractions (assessed by SDS-PAGE) were pooled and imidazole was then buffer exchanged and concentrated with 3 kDa MWCO centrifugal

concentrator. Protein concentration was assessed by A_{280}, correction for extinction coefficient. Purity was determined by SDS-PAGE, and α-His$_6$ western blot.

Western blot

15% SDS-PAGE gels were run with 1 μg of protein, and transferred to a PVDF membrane (0.2 μm pore size) for 1 hour at 4°C, using a wet transfer tank (Trans-blot, Bio Rad). The membrane was rinsed with deionized (DI) water and blocked with 2% non-fat dry milk (Lab Scientific #978-907-4243) in tris buffered saline with 0.1% Tween-20 (TBST) for 30 minutes at room temperature (RT). Blots were stained with 1:10,000 α-His$_6$-HRP (Invitrogen, MA1-80218) in blocking buffer overnight at 4°C. Blots were then washed with PBST three times for 5 minutes each. Signal was developed using SuperSignal Western Pico PLUS (Thermo Scientific) chemiluminescent substrate according to the manufacturer's instructions and visualized on an ImageQuant LAS 4000.

Size exclusion chromatography (SEC)

SEC was performed on a HiLoad 16/600 Superdex 75 pg (Cytiva) column on an ÄKTApurifier FPLC (GE) system. Sterile filtered and degassed 10 mM Tris HCl, 300 mM NaCl, 10 % glycerol, pH 7.8 was used as a mobile phase and was run at 0.8 mL/min at 4°C. Data was collected with Unicorn 5.31 (GE).

Native polyacrylamide gel electrophoresis (PAGE)

15% polyacrylamide gels were cast with 3.5 mL 30% acrylamide:0.8% bis-acrylamide, 1.7mL of 1.5 M Tris HCl buffer, 70 μL of 10% ammonium persulfate, and 7 μL of TEMED per gel. To analyze the dimerization of CFP10 and ESAT6, 25 μM stocks of each protein were made, mixed in varying ratios, and incubated for 60 minutes at 4 C. Non-denaturing loading buffer was added and reactions were loaded then run at 4°C overnight at 50 V in Tris-Glycine buffer without SDS (National Diagnostics) and then Coomassie stained.

Hemolysis

Bacterial hemolysis

Hemolysis experiments were performed as described previously (Conrad et al., 2017). Sheep blood (HemoStat labs, SBC100) was washed with PBS by centrifugation at 3200×g for 5 minutes and resuspended to a final concentration of 1% (v/v) red blood cells (RBC) in PBS. Bacterial cultures, Mm, Mtb, MtbΔRD1 were grown in Middlebrook 7H9 with OADC to an OD_{600} between 0.3 and 1.0. Cultures were washed with PBS by centrifugation at 500×g for 5 minutes and resuspended in PBS. The equivalent of 3 mL of culture at OD_{600} 1.0 was resuspended in 100 µL of PBS and combined with 100 µL of 1% RBCs. Centrifuged samples at 3200×g for 5 minutes, then incubated the pelleted samples at 37°C for Mtb and MtbΔRD1, or 33°C for Mm for 2 hours. Samples were then resuspended by pipette and spun again similarly. The absorbance at 405 nm was measured for each sample using a plate reader, as well as for samples without bacteria and samples with 0.1% Triton-X100. Percent hemolysis was calculated as (A_{405}Sample − A_{405}PBS) ÷ (A_{405}Triton − A_{405}PBS) × 100.

Protein hemolysis

For measurement of protein hemolysis, RBCs were resuspended to 1% (v/v) in McIlvaine buffer of pH 4.5, 5.5, 6.5, 7.5, and 8.5 prepared as previously described (McIlvaine, 1921). 100 µL of 1 mg/mL ESAT-6 was combined with 100 µL of 1% RBC solution and incubated at RT for 1 hour. Samples were then spun at 3200×g for 5 minutes and the A_{405} supernatants were measured by plate reader. PBS and Triton samples were prepared similarly to bacterial hemolysis, and % hemolysis was calculated using the same formula.

Biolayer interferometry (BLI)

BLI was performed using an Octet Red384 machine (ForteBio). Octet Streptavidin Biosensors (Sartorius, #18-5019) were used for all experiments. Biotinylated proteins were

prepared using the succinimide (ESAT-6, CFP-10, RBD) or sortase (ESAT-6-LPETG, E11rv, VHH 52) method. Recombinant SARS-Cov-2 spike RBD was used as a loading control for ESAT-6 and CFP-10 experiments, while VHH 52 against influenza was used as a loading control for E11rv experiments. For all experiments, Biosensors were soaked for 20 minutes in DI water, blocked for 30 seconds in 10mM Citrate, 100mM NaCl, 3mM EDTA, 0.1% BSA, 0.005% Tween-20 (running buffer) which was adjusted to match the pH of the test condition (4.5, 5.0, 5.5, 6.0, or 7.5). Biotinylated protein was then loaded onto the biosensors until approximately 1 nm of binding response was observed. Excess protein was washed off with three cycles of 15 seconds in 10 mM glycine pH 1.7 then 15 seconds in running buffer. Washing was followed by a 30 second baseline step in running buffer, an association step with test analyte diluted in running buffer, then dissociation step in plain running buffer. When multiple conditions were tested, the lowest concentration was tested first, and 3 wash cycles were performed between conditions. Loading control biosensors followed the same protocol with identical sample concentrations. Data was collected with Octet Data Acquisition 10.0.0.87 (ForteBio), and data was analyzed with Octet Data Analysis HT 10.0.0.48 (ForteBio). Background subtraction was performed using loading control biosensors, data was aligned to the average of the baseline step, and smoothed by Savitzky-Golay filtering. All data were fit to a 1:1 model using the "full (assoc and dissoc) setting" using the entire step length. Reported kinetic binding constants (K_D, K_{ON}, and K_{OFF}) values were calculated by taking the geometric mean of binding constants calculated for individual conditions and replicates. Conditions were excluded from the average when the Data Analysis HT software was unable to calculate all constants for a given condition due to insufficient signal. The only conditions excluded using this criterion were ESAT-6 pH 7.5 self-association at 0.316 nM, and E11rv association with ESAT-6 and ESAT-6-LPETG at 0.33 and 0.1 μM.

Turbidity assay

ESAT-6 was buffer exchanged into PBS using a Zeba spin column (ThermoFisher) and diluted to a concentration of 50 µM. 30 µL of ESAT-6 was added to each well in a 384 well plate. To each well, 2 µL of either PBS or Citrate buffer was added. Citrate buffer contained 50mM citric acid and 100 mM NaCl, and was adjusted for pH such that mixing 5mL buffer with 45mL PBS resulted in a solution with pH 4.5. Plates were immediately added to a plate reader following pH adjustment and A_{350} was read every 2 minutes for a total of 60 minutes with 10 seconds of shaking between each read. Turbidity was calculated as A_{350}Sample − A_{350}PBS.

Biotinylation

Succinimide biotinylation

Recombinant ESAT-6, CFP-10, and RBD (lacking an LPETG tag) were biotinylated using the ChromaLINK biotinylation kit (Vector labs). Manufacturer's instructions were used. 3 molar equivalents of biotinylation reagent yielded a labeling level of 0.99 biotins/protein calculated using the E1% method in the manufacturer's labeling calculator. Proteins were buffer exchanged into PBS by passing through a PBS-equilibrated Zeba desalting column (ThermoFisher, 89882). Protein aliquots were snap frozen in liquid nitrogen and stored at -80°C until use.

Sortase biotinylation

ESAT-6-LPETG and LPETG-tagged nanobodies were C-terminally biotinylated using sortase as previously described (Guimaraes et al., 2013; Popp et al., 2009). Briefly, 20 µL of 20 mg/mL sortase enzyme, 20 µL of 10 mM GGG-Biotin peptide, and 200 µL of 1mg/mL LPETG-labeled protein. This mixture was incubated at 4°C overnight, then added to 50 uL of packed, PBS-washed Ni-NTA beads to remove the His-tagged sortase enzyme and any unreacted protein for 2 hours at 4°C. The resulting supernatant was buffer exchanged into PBS by passing

through a PBS-equilibrated Zeba desalting column (ThermoFisher, 89882). Protein aliquots were snap frozen in liquid nitrogen and stored at -80°C until use.

Protein microscopy

Coverslips were coated in poly-L-Lysine at 4°C overnight, washed once with PBS, then dried before use. A 9:1 molar ratio of ESAT-6:ESAT-6-LPETG-Biotin (final concentration 0.24 mg/mL) was prepared prior to addition of 10× citrate buffer prepared similarly to the turbidity assay. The guanidine-containing sample used a protein concentration of 0.7 mg/mL and included a final concentration of 2M guanidine. The treated protein mixtures were incubated at RT for 30 minutes. Five 2μL drops were added to each coverslip and incubated at RT for 30 minutes. Coverslips were fixed by addition of 4% formaldehyde in PBS for 30 minutes at RT, washed three times with PBS, blocked in 2.5% BSA in PBS for 30 minutes at RT, washed 3 times with PBS, stained with 1:10,000 (in PBS) streptavidin-AF488 (Jacskon Immuno, 016-540-084), and finally washed 3 times with PBS. Coverslips were mounted onto microscope slides with Prolong Gold antifade (ThermoFisher, P10144). Images were captured on a Zeiss LSM 980 with Airyscan2 using a 63× oil objective and processed with Zeiss Blue Airyscan joint deconvolution.

Size exclusion chromatography multi-angle light scattering (SEC-MALS)

SEC-MALS was performed on an AKTApure FPLC (Cytiva) with a DAWN MALS detector (Wyatt). 100 μg of ESAT-6 was buffer exchanged with a Zeba spin column immediately prior to each experiment and injected onto a Superdex 75 increase 10/300 column at a flow rate of 0.5 mL/min at 4°C. The mobile phase was 10 mM Citrate, 300 mM NaCl, pH 4.5 or pH 7.5. Buffers were sterile filtered to 0.1 μm and degassed prior to use. Data analysis was performed using ASTRA 8.1.2.1 (Wyatt).

Modeling

Homology Modeling

The ESAT6 and CFP10 protein sequences were modeled via the Homology Modeling protocol in YASARA version 22.09.24. Sidechain optimization occurred through the FoldX plugin, with an energy minimization using AMBER14 force-field. X-ray structures with specified PDB IDs: 3FAV-A, 4J11-B, 4J7K-B, 4J10-A and 4J7J-B (PDB ID-Chain) served as templates for full-length modeling of both proteins, with alternative models considered if alignments were unclear. For CFP10, about 66% aligned with the template, and specific residues (MAEMKTDAAT and RADEEQQQAL) were predicted using loop modeling. Similarly, around 69% of ESAT6 aligned, with residues (STEGNVTGMF and MTEQQW) modeled as described earlier. After side-chain building and optimization, new model components underwent combined steepest descent and simulated annealing minimization. YASARA then integrated the best model parts to create a high-accuracy hybrid for each protein. Structures, dihedrals, and 1D to 3D packing were inspected for optimal monomer models. Dimer models were based on orientations from the 3FAV template, while tetrameric structures were predicted using dimer models as templates via the M-Zdock server.

Molecular Dynamic Simulations

The protonation status of amino acid residues and subsequent alteration of side-chain interactions and the domain structure can be influenced by the pH, impacting the stability, dynamics, and/or interactions of CFP10, ESAT6, and their heterodimers. As such, these were examined at both pH 4.5 and 7.4 through molecular dynamics simulations. These simulations, performed under the NPT ensemble with periodic boundary conditions, provided a sampling of the conformational space available to the various oligomeric forms of ESAT6 and CFP10. The domains were subjected to MD simulations for a period of 50 ns and snapshots were taken at 250 ps intervals for later examination. Each simulation process was run twice with distinct

random seeds to confirm the reliability of the simulations. The RMSF of each simulation was plotted as displayed in the Figure.

Nanobody discovery

Nanobody discovery was performed as previously described (Weinstein et al., 2022). Briefly, Alpacas were immunized with recombinant ESAT-6 protein and immune serum was collected. Peripheral blood mononuclear cells (PBMC) were isolated and RNA was extracted with an RNeasy mini kit (Qiagen 74104), which was then converted to cDNA using Superscript III (Invitrogen 18080051). VHH genes were amplified using gene specific primers for long- and shot-hinge heavy-chain-only antibodies (Maass et al., 2007). Amplified VHH genes were cloned into a phagemid vector based on pCANTAB-5E and transformed into competent TG1 *E. coli*. The bacterial library was infected with helper phage to generate a phage library and purified by PEG precipitation (Frei and Lai, 2016). The phage library which was panned against recombinant ESAT-6 to enrich strong binders. Panning consisted of incubating the purified phage library in antigen-coated tubes and then eluting with pH 2.2 glycine. Eluted phage were neutralized with 1M Tris pH 9.1, and transferred to log-phase ER2738 *E. coli*, to produce the enriched library, which was plated on agar. Individual ER2738 clones were selected and screened by ELISA to quantify affinity. E11rv was selected for further testing based on its performance in the screening ELISA, and was cloned into the pHEN periplasmic expression plasmid.

Nanobody purification

Nanobodies were purified by periplasmic purification. pHEN plasmid containing each nanobody was transformed into *E. coli* WK6 competent cells. 20 mL starter cultures were grown overnight at 37 C with shaking in Terrific Broth (2% tryptone, 1% yeast extract, 90mM phosphate) with 100 ug/mL ampicillin to stationary phase. Starter cultures were used to begin 1L Terrific Broth cultures to be grown at 37C. When cultures reached OD600 of approximately

0.6 OD, they were induced with 1 mM IPTG overnight at 30 C. Bacteria was pelleted at 4,000 xg for 10 minutes and resuspended in 40 mLs of lysis buffer (200 mM HEPES, 0.65 mM EDTA, 0.5 M sucrose, at cold pH 8), then incubated at 4C for 1-2 hrs. Add 40 mLs of ice cold water and incubate for 2 hrs, rotating, to lyse periplasm by osmotic shock. Periplasmic fraction was isolated by centrifuging lysate at 8,000 xg for 15 minutes, twice. VHH E11 was purified with Ni-NTA chromatography. Purified E11 was then buffer exchanged and concentrated with 3kDa cutoff centrifuge filters (Millipore), then aliquoted and frozen for future use.

Enzyme linked immunosorbent assay (ELISA)

ELISA experiments were performed as described previously (Weinstein et al., 2022). MaxiSorp plates (Invitrogen 442404) were coated with ESAT-6 at 5 µg/mL in PBS overnight at 4°C. Plates were blocked in 2% BSA, 2% Polyvinylpyrrolidone (PVP), 0.1% Tween-20 in PBS (blocking buffer) for 30 minutes at RT. Dilutions of E11rv or isotype control VHH 52 were made in blocking buffer and added to plates for 1 hour at RT with shaking. Plates were washed with PBST 3 times for 5 minutes each and biotinylated anti-VHH antibody (Jackson Immuno 128-065-232) at 1:10,000 in blocking buffer was added for 1 hour at RT with shaking. Plates were washed again and incubated with 1:10,000 streptavidin-HRP (Jackson Immuno 016-030-084) in blocking buffer for 1 hour at RT. Plates were washed again and incubated with 50 µL of ODP (ThermoFisher 34006), prepared according to the manufacturer's instructions, for 15 minutes before stopping with 50 µL of 2N H_2SO_4. A_{492} was measured using a CLARIOstar PLUS (BMG) plate reader. Raw data was background subtracted with wells lacking nanobody and normalized by dividing by the highest binding well, then fit to a 4PL sigmoid curve in Prism 10.0.0 (Graphpad) to determine the EC_{50}.

Hydrogen-deuterium exchange (HDX)

HDX-MS sample preparation

HDX reactions comparing ESAT6 Apo to E11rv-bound were carried out in 30 µl reaction volumes containing 15 pmol of ESAT6. A protein mastermix was created for both reaction conditions (500 nM ESAT6, 1 µM E11rv or equivalent volume of E11rv buffer). The exchange reactions were initiated by the addition of 25 µL of D_2O buffer (20 mM HEPES pH 7.5, 100 mM NaCl) to 5 µL of protein mastermix (final D_2O concentration of 78.6% [v/v]). Reactions proceeded for 0.3s (3s on ice), 3s, 30s, 300s, and 3000s at 20°C before being quenched with ice cold acidic quench buffer, resulting in a final concentration of 0.6M guanidine HCl and 0.9% formic acid post quench. All conditions and timepoints were created and run in independent triplicate. Samples were flash frozen immediately after quenching and stored at -80°C until injected onto the ultra-performance liquid chromatography (UPLC) system for proteolytic cleavage, peptide separation, and injection onto a QTOF for mass analysis, described below.

Protein digestion and MS/MS data collection

Protein samples were rapidly thawed and injected onto an integrated fluidics system containing a HDx-3 PAL liquid handling robot and climate-controlled (2°C) chromatography system (LEAP Technologies), a Dionex Ultimate 3000 UHPLC system, as well as an Impact HD QTOF Mass spectrometer (Bruker). The full details of the automated LC system are described in (Stariha et al., 2021). The samples were run over one immobilized pepsin column (Waters; Enzymate Protein Pepsin Column, 300Å, 5µm, 2.1 mm X 30 mm) at 200 µL/min for 3 minutes at 2°C. The resulting peptides were collected and desalted on a C18 trap column (Acquity UPLC BEH C18 1.7mm column (2.1 x 5 mm); Waters 186003975). The trap was subsequently eluted in line with an ACQUITY 1.7 µm particle, 100 × 1 mm^2 C18 UPLC column (Waters), using a gradient of 3-35% B (Buffer A 0.1% formic acid; Buffer B 100% acetonitrile) over 11 minutes immediately followed by a gradient of 35-80% over 5 minutes. Mass spectrometry experiments

acquired over a mass range from 150 to 2200 m/z using an electrospray ionization source operated at a temperature of 200°C and a spray voltage of 4.5 kV.

Peptide identification

Peptides were identified from a non-deuterated sample of ESAT6 using data-dependent acquisition following tandem MS/MS experiments (0.5 s precursor scan from 150-2000 m/z; twelve 0.25 s fragment scans from 150-2000 m/z). MS/MS datasets were analysed using PEAKS7 (PEAKS), and peptide identification was carried out by using a false discovery-based approach, with a threshold set to 0.1% using a database of purified proteins and known contaminants. The search parameters were set with a precursor tolerance of 20 ppm, fragment mass error 0.02 Da, charge states from 1-8, leading to a selection criterion of peptides that had a -10logP score of 16.2.

Mass Analysis of Peptide Centroids and Measurement of Deuterium Incorporation

HD-Examiner Software (Sierra Analytics) was used to automatically calculate the level of deuterium incorporation into each peptide. All peptides were manually inspected for correct charge state, correct retention time, appropriate selection of isotopic distribution, etc. Deuteration levels were calculated using the centroid of the experimental isotope clusters. Results are presented as relative levels of deuterium incorporation and the only control for back exchange was the level of deuterium present in the buffer (78.6%). Differences in exchange in a peptide were considered significant if they met all three of the following criteria: ≥4.5% change in exchange, ≥0.45 Da difference in exchange, and a p value <0.01 using a two tailed student t-test. Samples were only compared within a single experiment and were never compared to experiments completed at a different time with a different final D_2O level. The data analysis statistics for all HDX-MS experiments are in **Supplemental Table 1** according to the guidelines of (Masson et al., 2019). The mass spectrometry proteomics data have been deposited to the ProteomeXchange Consortium via the PRIDE partner repository (Perez-Riverol et al., 2022).

Cell lines

Human THP-1 monocytes (ATCC catalog no. TIB-22) were cultured in RPMI medium with 10% FBS (Seradigm) and 1% penicillin-streptomycin (Gibco) at 37°C and 5% CO_2. Cultures were routinely monitored for mycoplasma contamination (abm). Authenticated THP-1 cells were obtained from ATCC; no additional authentication was performed.

Imaging-based Mtb viability assay

Live/Dead H37rv Mtb constitutively express mCherry and have Tet[ON] inducible GFP expression. THP-1 cells were seeded at 40,000 cells/well in glass bottom, black-walled 96 well tissue culture plates and treated with 100 µM Phorbol-12-myristate-13-acetate (PMA) for 24 hours prior to infection. Endotoxin free E11rv and unrelated isotype nanobodies were prepared to 1 mg/mL and sterile filtered prior to use. THP-1 cells were infected at an MOI of 1 with Live/Dead Mtb was pre-incubated for 30 minutes with 100 µg/mL of nanobody. Infected plates were incubated for 3 days in tissue culture conditions. Doxycyline was added to a final concentration of 1 µg/mL and incubated for 24 hours. Plates were fixed with 5% formaldehyde in PBS for 1 hour at RT in accordance with OHSU biosafety procedures before removing plates from the BSL3. Plates were then washed with PBS and stained with Phalloidin-AF405 at 1:40 from 6.6 µM stock for 1 hour. Wells were imaged with a Keyence (BZX-710) using a 20× S Plan Fluor ELWD lens. 49 images were captured for each well using the same exposure settings for each experiment. Images were analyzed with CellProfiler 4.2.5 (Stirling et al., 2021). Images with obvious defects such as large dust particles were excluded from the analysis. Mean GFP / Mean RFP was calculated for each identified TB particle and the average GFP/RFP value was tabulated for each image. Images were plotted as individual points in Prism (Graphpad) as described in the statistics section.

Continuous luminescence viability assay

THP-1 cells were transduced with lentivirus to express nanobody-GFP fusion constructs for E11rv and VHH 52 under a Tet^{ON} promoter (pInducer20 plasmid). The lentiviruses were generated as described previously (Niekamp et al., 2021). THP-1 cells were transduced and selected with 600 µg/mL of G418 for 3 weeks, then maintained with 300 µg/mL G418 in every other passage. For each experiment opaque white 96-well plates were seeded with 30,000 cells/well along with a matched clear plate, both including 100 nM PMA. Cells were incubated with PMA for 24 hours before inducing with 1 µg/mL doxycycline for another 24 hours. Cell health and nanobody expression was verified by microscopy of the clear plate. The opaque plate was infected with bioluminescent pLux Mtb, which expresses the full luxABCDE cassette, at an MOI of 1. The plate was sealed with a Beathe-Easy plate seal (Research Products International 248738) and put into a climate-controlled CLARIOstart plate reader for continuous luminescence reading for 120 hours.

Statistics

Statistical analysis was performed in Prism 10.0.0 (Graphpad). In Figure 2B, two-tailed one sample t-tests were performed with a significance cutoff of 0.05 against a hypothetical value of 0. In figure 7B, a two-tailed unpaired t test was performed with a significance cutoff of 0.05. For all plots, * = 0.05, ** = 0.01, *** = 0.001, **** = 0.0001.

Figure legends

Figure 1: Expression of recombinant ESAT-6 and CFP-10. (A) amino acid sequences derived from plasmid sequencing of pMRLB.7 (ESAT-6) and pMRLB.46 (CFP-10) plasmids available from BEI Resources. The yellow highlights indicate the expected FALE-Histidine tag amino acid sequence while the blue highlights indicate unexpected additional amino acids. (B)

SDS-PAGE gel of purified ESAT-6 and CFP-10 with a paired anti-His$_6$ western blot. (C) Size exclusion chromatography traces showing the retention volumes of purified ESAT-6, CFP-10 and an equimolar mixture of both (Dimer).

Figure 1 – figure supplement 1: Sequencing. (A) Sanger sequencing of pMRLB.7 with the ESAT-6 open reading frame (ORF) highlighted grey. (B) Sanger sequencing of pMRLB.46 with the CFP-10 ORF highlighted grey.

Figure 1 – figure supplement 2: Whole protein mass spectrometry (MS) of recombinant ESAT-6 and CFP-10. (A) Deconvoluted mass spectrum of recombinant ESAT-6 MS run. (B) Deconvoluted mass spectrum of recombinant CFP-10 MS run. (C) Computed mass of each protein compared with the measured masses. Fractional abundance combined the main peak with the harmonic artifact at twice the mass and gives an approximate relative proportion of each molecule in the sample. ESAT-6 is approximately 38% demethionylated while CFP-10 is fully demethionylated.

Figure 1 – source data 1: SDS-PAGE and Western blot. (A) Uncropped SDS-PAGE gel showing recombinant ESAT-6 and CFP-10 next to a BLUEstain 2 (Gold Bio) protein ladder and stained with Blazin' Blue (Goldbio) protein gel stain. (B) Uncropped western blot showing recombinant ESAT-6 and CFP-10 using a His-tag specific antibody.

Figure 2: functional testing of ESAT-6 and CFP-10. (A) Native-PAGE analysis of ESAT-6 and CFP-10 showing 1:1 complex formation at neutral pH. The displayed gel is representative of 3 replicates. (B) Contact-dependent red blood cell (RBC) hemolysis by whole bacteria, either *Mycobacterium marinum* (Mm), *Mycobacterium tuberculosis* (Mtb), or Mtb with the region of difference 1 deletion, incapable of producing ESAT-6 or CFP-10 (MtbΔRD1). Data in B represents 6 replicates. Statistical significance was determined using a one sample t test against a theoretical mean of 0. * = 0.05, ** = 0.01, *** = 0.001, **** = 0.0001.

Figure 2 – figure supplement 1: Hemolysis by recombinant ESAT-6. (A) Sheep red blood cell hemolysis assay carried out with purified ESAT-6 in citrate buffer at various pH values. Percent hemolysis was calculated by subtracting buffer background and dividing by Triton-X100 detergent lysed samples.

Figure 2 – source data 1: Native PAGE. (A) Native PAGE gel showing pure ESAT-6 on the left, pure CFP-10 on the right, and mixtures of both in the indicated ratios. The gel was stained with Blazin' Blue (Goldbio) protein gel stain.

Figure 3: Binding kinetics of ESAT-6 and CFP-10 under neutral and acidic conditions. (A) Biolayer interferometry (BLI) experimental design. Biotinylated ESAT-6 or CFP-10 are attached to streptavidin coated biosensors, then dipped into solutions of free ESAT-6 or CFP-10. (B) BLI experiment depicting ESAT-6 and CFP-10 association, ESAT-6 self-association, and CFP-10 self-association at pH 7.5 with 50 μM. BLI experiment showing (C) ESAT-6 self-association at pH 7.5, (D) CFP-10/ESAT-6 association at pH 7.5, (E) ESAT-6 self-association at pH 4.5, and (F) CFP-10/ESAT-6 association at pH 4.5 Proteins in (C-F) were tested at 1, 3.16, 10, 31.6, and 100 μM. (G) Table of apparent binding constants calculated with a 1:1 model for each indicated condition. (H) BLI experiment testing ESAT-6 self-association at pH 4.5, 5.0, 5.5, and 6.0 with 100 μM protein.

Figure 4: Extensive self-association of ESAT-6. (A) BLI long-association experiment showing 50 μM ESAT-6 at pH 4.5 or 7.5 attaching to biosensors coated with either ESAT-6 or CFP-10. (B) Turbidity assay showing 50 μM ESAT-6 or 50 μM CFP-10 at pH 4.5 or 7.5 over time. Absorbance at 350nm read every 2 minutes. (C) Lysine-labeled Biotinylated ESAT-6 has an average of 1 biotin per protein attached to the N-terminus or one of the orange highlighted lysine residues. The ESAT-6-LPETG construct amino acid sequence is shown which includes and inserted LPETG motif, in orange. Reaction with biotinylated poly-glycine via sortase-

mediated transpeptidation results in the teal highlighted residues being removed and replaced with a biotin molecule. BLI experiments at (D) pH 7.5 and (E) pH 4.5 showing unmodified soluble ESAT-6 interacting with streptavidin biosensor tips loaded with ESAT-6-Lysine-Biotin (red) or ESAT-6-LPETG-Biotin (blue). Curves were normalized by dividing response values by the amount of protein added during the loading step. (F) Summary of apparent kinetic binding constants in (D-E).

Figure 5: Stoichiometry of ESAT-6 self-interaction. (A) Fluorescence microscopy showing fluorescently labeled ESAT-6 complexes under different conditions: pH 4.5, pH 7.5, and pH 4.5 + 6M guanidine. The images shown are representative of 3 replicates. Size exclusion chromatography followed by multi-angle light scattering (SEC-MALS) traces showing UV absorbance, refractive index (dRI), and MALS data along with calculated molar mass over the peak at pH 7.5 (B), and pH 4.5 (C). Data in (B-C) is representative of 3 replicates. (D-F) Modeling of ESAT-6 in monomeric (D), homodimeric (E), and homotetrameric form (F). Hydrophobic residues are in yellow, polar residues are in blue, basic residues are in cyan, and acidic residues are in red. Key side chain residues are shown as spheres. (G) Root mean square fluctuation (RMSF) values are shown per residue for ESAT-6 monomer, dimer, and trimer at pH 7.5 and 4.5.

Figure 6: An ESAT-6-binding alpaca nanobody. (A) ELISA experiment on ESAT-6-coated plates showing nanobody E11rv and an irrelevant isotype control. E11rv displays an EC50 of 17.5 (95% CI 16.0-19.4) µg/mL. (B) BLI experiments with E11rv-coated biosensors tested against pMRLB.7 ESAT-6 (blue) or ESAT-6-LPETG (red) at 10, 3.3, 1, and 0.3 µM. (C) Summary of kinetic binding constants from (B). (D) schematic diagram of hydrogen-deuterium exchange (HDX) experiment showing apo ESAT-6 or E11rv-bound ESAT-6 incubated in D20, then subjected to digestion and mass spectrometry to measure the levels of deuterium incorporation at different times for different peptides, then mapping this to the protein sequence

to identify areas with less or greater deuterium exchange between the apo and bound conditions. (E) HDX data for ESAT-6 and E11rv showing reduced deuterium uptake around residue 50 and increased uptake around residue 75. (F) HDX shifts mapped to the ESAT-6 structure (PDB: 3FAV).

Figure 7: E11rv inhibits Mtb growth in cells. (A) representative fluorescence microscopy images for E11rv and isotype treated cultures. Results include data from 3 replicates. (B) Cellular assay testing the effect of infecting THP-1 cells with Live/Dead Mtb in the presence of E11rv for 3 days, treated with doxycycline for 24 hours to induce GFP expression by remaining metabolically active Mtb. The GFP/RFP ratio was calculated for each Mtb spot identified by fluorescence microscopy. Statistical significance was determined with a two-tailed unpaired t test. * = 0.05, ** = 0.01, *** = 0.001, **** = 0.0001. (C) Luminescence growth assay of stably transfected THP-1 cells expressing E11rv or isotype nanobody in their cytoplasm. Cells were infected with luminescent Mtb and monitored by luminescence plate reader for 120 hours. Results are representative of 6 replicates.

References Cited:

Aguilera, J., Karki, C.B., Li, L., Reyes, S.V., Estevao, I., Grajeda, B.I., Zhang, Q., Arico, C.D., Ouellet, H., Sun, J., 2020. Nα-Acetylation of the virulence factor EsxA is required for mycobacterial cytosolic translocation and virulence. J. Biol. Chem. 295, 5785–5794. https://doi.org/10.1074/jbc.RA119.012497

Alfadhli, A., Romanaggi, C., Barklis, R.L., Merutka, I., Bates, T.A., Tafesse, F.G., Barklis, E., 2021. Capsid-specific nanobody effects on HIV-1 assembly and infectivity. Virology 562, 19–28. https://doi.org/10.1016/j.virol.2021.07.001

Andersen, P., Andersen, A.B., Sørensen, A.L., Nagai, S., 1995. Recall of long-lived immunity to Mycobacterium tuberculosis infection in mice. J Immunol 154, 3359–3372.

Andreu, N., Zelmer, A., Fletcher, T., Elkington, P.T., Ward, T.H., Ripoll, J., Parish, T., Bancroft, G.J., Schaible, U., Robertson, B.D., Wiles, S., 2010. Optimisation of Bioluminescent Reporters for Use with Mycobacteria. PLoS One 5, e10777. https://doi.org/10.1371/journal.pone.0010777

Augenstreich, J., Arbues, A., Simeone, R., Haanappel, E., Wegener, A., Sayes, F., Chevalier, F.L., Chalut, C., Malaga, W., Guilhot, C., Brosch, R., Astarie-Dequeker, C., 2017. ESX-1 and phthiocerol dimycocerosates of Mycobacterium tuberculosis act in concert to cause

phagosomal rupture and host cell apoptosis. Cellular Microbiology 19, e12726. https://doi.org/10.1111/cmi.12726

Augenstreich, J., Haanappel, E., Sayes, F., Simeone, R., Guillet, V., Mazeres, S., Chalut, C., Mourey, L., Brosch, R., Guilhot, C., Astarie-Dequeker, C., 2020. Phthiocerol Dimycocerosates From Mycobacterium tuberculosis Increase the Membrane Activity of Bacterial Effectors and Host Receptors. Frontiers in Cellular and Infection Microbiology 10.

Bachran, C., Schröder, M., Conrad, L., Cragnolini, J.J., Tafesse, F.G., Helming, L., Ploegh, H.L., Swee, L.K., 2017. The activity of myeloid cell-specific VHH immunotoxins is target-, epitope-, subset- and organ dependent. Sci Rep 7, 17916. https://doi.org/10.1038/s41598-017-17948-0

Behura, A., Mishra, Abtar, Chugh, S., Mawatwal, S., Kumar, A., Manna, D., Mishra, Amit, Singh, R., Dhiman, R., 2019. ESAT-6 modulates Calcimycin-induced autophagy through microRNA-30a in mycobacteria infected macrophages. Journal of Infection 79, 139–152. https://doi.org/10.1016/j.jinf.2019.06.001

Bosserman, R.E., Nicholson, K.R., Champion, M.M., Champion, P.A., 2019. A New ESX-1 Substrate in Mycobacterium marinum That Is Required for Hemolysis but Not Host Cell Lysis. J Bacteriol 201. https://doi.org/10.1128/JB.00760-18

Canton, J., Khezri, R., Glogauer, M., Grinstein, S., 2014. Contrasting phagosome pH regulation and maturation in human M1 and M2 macrophages. Mol Biol Cell 25, 3330–3341. https://doi.org/10.1091/mbc.E14-05-0967

Carlsson, F., Joshi, S.A., Rangell, L., Brown, E.J., 2009. Polar Localization of Virulence-Related Esx-1 Secretion in Mycobacteria. PLOS Pathogens 5, e1000285. https://doi.org/10.1371/journal.ppat.1000285

Chen, J.M., Boy-Röttger, S., Dhar, N., Sweeney, N., Buxton, R.S., Pojer, F., Rosenkrands, I., Cole, S.T., 2012. EspD is critical for the virulence-mediating ESX-1 secretion system in Mycobacterium tuberculosis. J Bacteriol 194, 884–893. https://doi.org/10.1128/JB.06417-11

Chen, Y., Xiao, J., Li, Y., Xiao, Y., Xiong, Y., Liu, Y., Wang, S., Ji, P., Zhao, G., Shen, H., Lu, S., Fan, X., Wang, Y., 2019. Mycobacterial Lipoprotein Z Triggers Efficient Innate and Adaptive Immunity for Protection Against Mycobacterium tuberculosis Infection. Frontiers in Immunology 9.

Choi, H.-H., Shin, D.-M., Kang, G., Kim, K.-H., Park, J.B., Hur, G.M., Lee, H.-M., Lim, Y.-J., Park, J.-K., Jo, E.-K., Song, C.-H., 2010. Endoplasmic reticulum stress response is involved in Mycobacterium tuberculosis protein ESAT-6-mediated apoptosis. FEBS Letters 584, 2445–2454. https://doi.org/10.1016/j.febslet.2010.04.050

Clemmensen, H.S., Knudsen, N.P.H., Rasmussen, E.M., Winkler, J., Rosenkrands, I., Ahmad, A., Lillebaek, T., Sherman, D.R., Andersen, P.L., Aagaard, C., 2017. An attenuated Mycobacterium tuberculosis clinical strain with a defect in ESX-1 secretion induces minimal host immune responses and pathology. Scientific Reports 7, 46666. https://doi.org/10.1038/srep46666

Collars, O.A., Jones, B.S., Hu, D.D., Weaver, S.D., Champion, M.M., Champion, P.A., 2023. An N-acetyltransferase required for EsxA N-terminal protein acetylation and virulence in Mycobacterium marinum. bioRxiv 2023.03.14.532585. https://doi.org/10.1101/2023.03.14.532585

Conrad, W.H., Osman, M.M., Shanahan, J.K., Chu, F., Takaki, K.K., Cameron, J., Hopkinson-Woolley, D., Brosch, R., Ramakrishnan, L., 2017. Mycobacterial ESX-1 secretion system mediates host cell lysis through bacterium contact-dependent gross membrane disruptions. Proc Natl Acad Sci U S A 114, 1371–1376. https://doi.org/10.1073/pnas.1620133114

Cronin, R.M., Ferrell, M.J., Cahir, C.W., Champion, M.M., Champion, P.A., 2022. Proteo-genetic analysis reveals clear hierarchy of ESX-1 secretion in Mycobacterium marinum. Proc Natl Acad Sci U S A 119, e2123100119. https://doi.org/10.1073/pnas.2123100119

de Jonge, M.I., Pehau-Arnaudet, G., Fretz, M.M., Romain, F., Bottai, D., Brodin, P., Honoré, N., Marchal, G., Jiskoot, W., England, P., Cole, S.T., Brosch, R., 2007. ESAT-6 from Mycobacterium tuberculosis dissociates from its putative chaperone CFP-10 under acidic conditions and exhibits membrane-lysing activity. J Bacteriol 189, 6028–6034. https://doi.org/10.1128/JB.00469-07

De Leon, J., Jiang, G., Ma, Y., Rubin, E., Fortune, S., Sun, J., 2012. Mycobacterium tuberculosis ESAT-6 exhibits a unique membrane-interacting activity that is not found in its ortholog from non-pathogenic Mycobacterium smegmatis. J Biol Chem 287, 44184–44191. https://doi.org/10.1074/jbc.M112.420869

Dong, H., Jing, W., Runpeng, Z., Xuewei, X., Min, M., Ru, C., Yingru, X., Shengfa, N., Rongbo, Z., 2016. ESAT6 inhibits autophagy flux and promotes BCG proliferation through MTOR. Biochemical and Biophysical Research Communications 477, 195–201. https://doi.org/10.1016/j.bbrc.2016.06.042

Eitson, J.L., Medeiros, J.J., Hoover, A.R., Srivastava, S., Roybal, K.T., Aínsa, J.A., Hansen, E.J., Gumbo, T., van Oers, N.S.C., 2012. Mycobacterial Shuttle Vectors Designed for High-Level Protein Expression in Infected Macrophages. Appl Environ Microbiol 78, 6829–6837. https://doi.org/10.1128/AEM.01674-12

Fan, Y., Tan, K., Chhor, G., Butler, E.K., Jedrzejczak, R.P., Missiakas, D., Joachimiak, A., 2015. EsxB, a secreted protein from Bacillus anthracis forms two distinct helical bundles. Protein Sci 24, 1389–1400. https://doi.org/10.1002/pro.2715

Frei, J.C., Lai, J.R., 2016. Protein and Antibody Engineering by Phage Display, in: Methods in Enzymology. Elsevier, pp. 45–87. https://doi.org/10.1016/bs.mie.2016.05.005

Gallegos, A.M., Pamer, E.G., Glickman, M.S., 2008. Delayed protection by ESAT-6–specific effector CD4+ T cells after airborne M. tuberculosis infection. Journal of Experimental Medicine 205, 2359–2368. https://doi.org/10.1084/jem.20080353

García-Nafría, J., Watson, J.F., Greger, I.H., 2016. IVA cloning: A single-tube universal cloning system exploiting bacterial In Vivo Assembly. Sci Rep 6, 27459. https://doi.org/10.1038/srep27459

Gey van Pittius, N.C., Gamieldien, J., Hide, W., Brown, G.D., Siezen, R.J., Beyers, A.D., 2001. The ESAT-6 gene cluster of Mycobacterium tuberculosis and other high G+C Gram-positive bacteria. Genome Biol 2, research0044.1-research0044.18.

Giglione, C., Boularot, A., Meinnel, T., 2004. Protein N-terminal methionine excision. Cell Mol Life Sci 61, 1455–1474. https://doi.org/10.1007/s00018-004-3466-8

Guimaraes, C.P., Witte, M.D., Theile, C.S., Bozkurt, G., Kundrat, L., Blom, A.E.M., Ploegh, H.L., 2013. Site-specific C-terminal and internal loop labeling of proteins using sortase-mediated reactions. Nat Protoc 8, 1787–1799. https://doi.org/10.1038/nprot.2013.101

Harris, N.J., Jenkins, M.L., Nam, S.-E., Rathinaswamy, M.K., Parson, M.A.H., Ranga-Prasad, H., Dalwadi, U., Moeller, B.E., Sheeky, E., Hansen, S.D., Yip, C.K., Burke, J.E., 2023. Allosteric activation or inhibition of PI3Kγ mediated through conformational changes in the p110γ helical domain. Elife 12, RP88058. https://doi.org/10.7554/eLife.88058

Harrison, D.E., Astle, C.M., Niazi, M.K.K., Major, S., Beamer, G.L., 2014. Genetically diverse mice are novel and valuable models of age-associated susceptibility to Mycobacterium tuberculosis. Immunity & Ageing 11, 24. https://doi.org/10.1186/s12979-014-0024-6

Hirel, P.H., Schmitter, M.J., Dessen, P., Fayat, G., Blanquet, S., 1989. Extent of N-terminal methionine excision from Escherichia coli proteins is governed by the side-chain length of the penultimate amino acid. Proceedings of the National Academy of Sciences 86, 8247–8251. https://doi.org/10.1073/pnas.86.21.8247
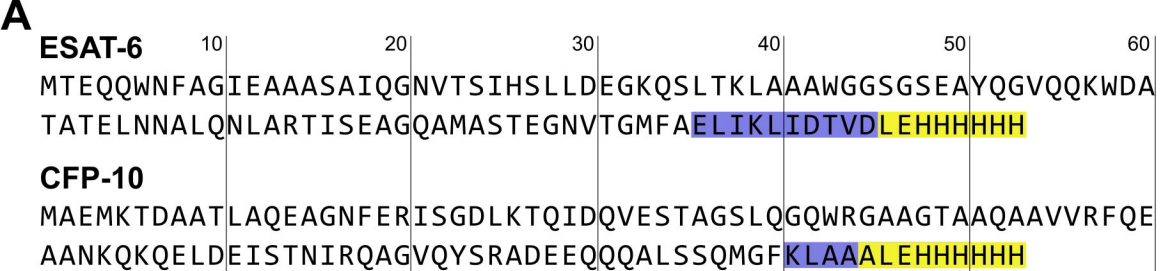
Hoogenboom, H.R., Griffiths, A.D., Johnson, K.S., Chiswell, D.J., Hudson, P., Winter, G., 1991. Multi-subunit proteins on the surface of filamentous phage: methodologies for displaying antibody (Fab) heavy and light chains. Nucleic Acids Res 19, 4133–4137. https://doi.org/10.1093/nar/19.15.4133

Houben, D., Demangel, C., van Ingen, J., Perez, J., Baldeon, L., Abdallah, A.M., Caleechurn, L., Bottai, D., van Zon, M., de Punder, K., van der Laan, T., Kant, A., Bossers-de Vries, R., Willemsen, P., Bitter, W., van Soolingen, D., Brosch, R., van der Wel, N., Peters, P.J., 2012. ESX-1-mediated translocation to the cytosol controls virulence of mycobacteria. Cell Microbiol 14, 1287–98. https://doi.org/10.1111/j.1462-5822.2012.01799.x

Houben, R.M.G.J., Dodd, P.J., 2016. The Global Burden of Latent Tuberculosis Infection: A Re-estimation Using Mathematical Modelling. PLOS Medicine 13, e1002152. https://doi.org/10.1371/journal.pmed.1002152

Jang, A.R., Choi, J.H., Shin, S.J., Park, J.H., 2018. Mycobacterium tuberculosis ESAT6 induces IFN-beta gene expression in Macrophages via TLRs-mediated signaling. Cytokine 104, 104–109. https://doi.org/10.1016/j.cyto.2017.10.006

Karki, C., Xian, Y., Xie, Y., Sun, S., Lopez-Hernandez, A.E., Juarez, B., Wang, J., Sun, J., Li, L., 2020. A computational model of ESAT-6 complex in membrane. J Theor Comput Chem 19, 2040002. https://doi.org/10.1142/s0219633620400027

Kinhikar, A.G., Verma, I., Chandra, D., Singh, K.K., Weldingh, K., Andersen, P., Hsu, T., Jacobs, W.R., Laal, S., 2010. Potential role for ESAT6 in dissemination of M. tuberculosis via human lung epithelial cells. Mol Microbiol 75, 92–106. https://doi.org/10.1111/j.1365-2958.2009.06959.x

Koo, I.C., Wang, C., Raghavan, S., Morisaki, J.H., Cox, J.S., Brown, E.J., 2008. ESX-1-dependent cytolysis in lysosome secretion and inflammasome activation during mycobacterial infection. Cell Microbiol 10, 1866–1878. https://doi.org/10.1111/j.1462-5822.2008.01177.x

Koyuncu, D., Niazi, M.K.K., Tavolara, T., Abeijon, C., Ginese, M.L., Liao, Y., Mark, C., Specht, A., Gower, A.C., Restrepo, B.I., Gatti, D.M., Kramnik, I., Gurcan, M., Yener, B., Beamer, G., 2021. CXCL1: A new diagnostic biomarker for human tuberculosis discovered using Diversity Outbred mice. PLOS Pathogens 17, e1009773. https://doi.org/10.1371/journal.ppat.1009773

Kumar, P., Agarwal, R., Siddiqui, I., Vora, H., Das, G., Sharma, P., 2012. ESAT6 differentially inhibits IFN-γ-inducible class II transactivator isoforms in both a TLR2-dependent and -independent manner. Immunology & Cell Biology 90, 411–420. https://doi.org/10.1038/icb.2011.54

Leddy, O., White, F.M., Bryson, B.D., 2023. Immunopeptidomics reveals determinants of Mycobacterium tuberculosis antigen presentation on MHC class I. eLife 12, e84070. https://doi.org/10.7554/eLife.84070

Lienard, J., Nobs, E., Lovins, V., Movert, E., Valfridsson, C., Carlsson, F., 2020. The Mycobacterium marinum ESX-1 system mediates phagosomal permeabilization and type I interferon production via separable mechanisms. Proc Natl Acad Sci U S A 117, 1160–1166. https://doi.org/10.1073/pnas.1911646117

Lightbody, K.L., Ilghari, D., Waters, L.C., Carey, G., Bailey, M.A., Williamson, R.A., Renshaw, P.S., Carr, M.D., 2008. Molecular features governing the stability and specificity of functional complex formation by Mycobacterium tuberculosis CFP-10/ESAT-6 family proteins. J Biol Chem 283, 17681–17690. https://doi.org/10.1074/jbc.M800123200

Lim, Y.-J., Yi, M.-H., Choi, J.-A., Lee, J., Han, J.-Y., Jo, S.-H., Oh, S.-M., Cho, H.J., Kim, D.W., Kang, M.-W., Song, C.-H., 2016. Roles of endoplasmic reticulum stress-mediated apoptosis in M1-polarized macrophages during mycobacterial infections. Sci Rep 6, 37211. https://doi.org/10.1038/srep37211

López-Jiménez, A.T., Cardenal-Muñoz, E., Leuba, F., Gerstenmaier, L., Barisch, C., Hagedorn, M., King, J.S., Soldati, T., 2018. The ESCRT and autophagy machineries cooperate to repair ESX-1-dependent damage at the Mycobacterium-containing vacuole but have opposite impact on containing the infection. PLOS Pathogens 14, e1007501. https://doi.org/10.1371/journal.ppat.1007501

Maass, D.R., Sepulveda, J., Pernthaner, A., Shoemaker, C.B., 2007. Alpaca (Lama pacos) as a convenient source of recombinant camelid heavy chain antibodies (VHHs). J Immunol Methods 324, 13–25. https://doi.org/10.1016/j.jim.2007.04.008

MacMicking, J.D., Taylor, G.A., McKinney, J.D., 2003. Immune Control of Tuberculosis by IFN-γ-Inducible LRG-47. Science 302, 654–659. https://doi.org/10.1126/science.1088063

Martin, C.J., Booty, M.G., Rosebrock, T.R., Nunes-Alves, C., Desjardins, D.M., Keren, I., Fortune, S.M., Remold, H.G., Behar, S.M., 2012. Efferocytosis is an innate antibacterial mechanism. Cell Host Microbe 12, 289–300. https://doi.org/10.1016/j.chom.2012.06.010

Masson, G.R., Burke, J.E., Ahn, N.G., Anand, G.S., Borchers, C., Brier, S., Bou-Assaf, G.M., Engen, J.R., Englander, S.W., Faber, J., Garlish, R., Griffin, P.R., Gross, M.L., Guttman, M., Hamuro, Y., Heck, A.J.R., Houde, D., Iacob, R.E., Jørgensen, T.J.D., Kaltashov, I.A., Klinman, J.P., Konermann, L., Man, P., Mayne, L., Pascal, B.D., Reichmann, D., Skehel, M., Snijder, J., Strutzenberg, T.S., Underbakke, E.S., Wagner, C., Wales, T.E., Walters, B.T., Weis, D.D., Wilson, D.J., Wintrode, P.L., Zhang, Z., Zheng, J., Schriemer, D.C., Rand, K.D., 2019. Recommendations for performing, interpreting and reporting hydrogen deuterium exchange mass spectrometry (HDX-MS) experiments. Nat Methods 16, 595–602. https://doi.org/10.1038/s41592-019-0459-y

Mba Medie, F., Champion, M.M., Williams, E.A., Champion, P.A.D., 2014. Homeostasis of N-α-Terminal Acetylation of EsxA Correlates with Virulence in Mycobacterium marinum. Infect Immun 82, 4572–4586. https://doi.org/10.1128/IAI.02153-14

McIlvaine, T.C., 1921. A BUFFER SOLUTION FOR COLORIMETRIC COMPARISON. Journal of Biological Chemistry 49, 183–186. https://doi.org/10.1016/S0021-9258(18)86000-8

Meerbrey, K.L., Hu, G., Kessler, J.D., Roarty, K., Li, M.Z., Fang, J.E., Herschkowitz, J.I., Burrows, A.E., Ciccia, A., Sun, T., Schmitt, E.M., Bernardi, R.J., Fu, X., Bland, C.S., Cooper, T.A., Schiff, R., Rosen, J.M., Westbrook, T.F., Elledge, S.J., 2011. The pINDUCER lentiviral toolkit for inducible RNA interference in vitro and in vivo. Proc Natl Acad Sci U S A 108, 3665–3670. https://doi.org/10.1073/pnas.1019736108

Mukherjee, P., Dutta, M., Datta, P., Dasgupta, A., Pradhan, R., Pradhan, M., Kundu, M., Basu, J., Chakrabarti, P., 2007. The RD1-encoded antigen Rv3872 of Mycobacterium tuberculosis as a potential candidate for serodiagnosis of tuberculosis. Clinical Microbiology and Infection 13, 146–152. https://doi.org/10.1111/j.1469-0691.2006.01660.x

Niazi, M.K.K., Dhulekar, N., Schmidt, D., Major, S., Cooper, R., Abeijon, C., Gatti, D.M., Kramnik, I., Yener, B., Gurcan, M., Beamer, G., 2015. Lung necrosis and neutrophils reflect common pathways of susceptibility to Mycobacterium tuberculosis in genetically diverse, immune-competent mice. Dis Model Mech 8, 1141–1153. https://doi.org/10.1242/dmm.020867

Niekamp, P., Guzman, G., Leier, H.C., Rashidfarrokhi, A., Richina, V., Pott, F., Barisch, C., Holthuis, J.C.M., Tafesse, F.G., 2021. Sphingomyelin Biosynthesis Is Essential for Phagocytic Signaling during Mycobacterium tuberculosis Host Cell Entry. mBio 12, e03141-20. https://doi.org/10.1128/mBio.03141-20

Okkels, L.M., Müller, E.-C., Schmid, M., Rosenkrands, I., Kaufmann, S.H.E., Andersen, P., Jungblut, P.R., 2004. CFP10 discriminates between nonacetylated and acetylated ESAT-6 of Mycobacterium tuberculosis by differential interaction. PROTEOMICS 4, 2954–2960. https://doi.org/10.1002/pmic.200400906
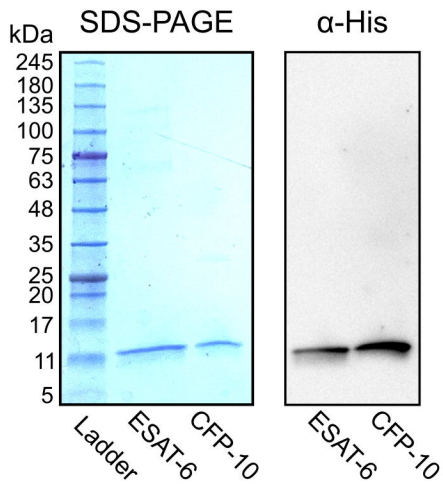
Osman, M.M., Shanahan, J.K., Chu, F., Takaki, K.K., Pinckert, M.L., Pagán, A.J., Brosch, R., Conrad, W.H., Ramakrishnan, L., 2022. The C terminus of the mycobacterium ESX-1 secretion system substrate ESAT-6 is required for phagosomal membrane damage and virulence. Proc Natl Acad Sci U S A 119, e2122161119. https://doi.org/10.1073/pnas.2122161119

Pathak, S.K., Basu, S., Basu, K.K., Banerjee, A., Pathak, S., Bhattacharyya, A., Kaisho, T., Kundu, M., Basu, J., 2007. Direct extracellular interaction between the early secreted antigen ESAT-6 of Mycobacterium tuberculosis and TLR2 inhibits TLR signaling in macrophages. Nat Immunol 8, 610–618. https://doi.org/10.1038/ni1468

Peng, H., Wang, X., Barnes, P.F., Tang, H., Townsend, J.C., Samten, B., 2011. The Mycobacterium tuberculosis Early Secreted Antigenic Target of 6 kDa Inhibits T Cell Interferon-γ Production through the p38 Mitogen-activated Protein Kinase Pathway. J Biol Chem 286, 24508–24518. https://doi.org/10.1074/jbc.M111.234062

Perez-Riverol, Y., Bai, J., Bandla, C., García-Seisdedos, D., Hewapathirana, S., Kamatchinathan, S., Kundu, D.J., Prakash, A., Frericks-Zipper, A., Eisenacher, M., Walzer, M., Wang, S., Brazma, A., Vizcaíno, J.A., 2022. The PRIDE database resources in 2022: a hub for mass spectrometry-based proteomics evidences. Nucleic Acids Res 50, D543–D552. https://doi.org/10.1093/nar/gkab1038

Popp, M.W., Antos, J.M., Ploegh, H.L., 2009. Site-specific protein labeling via sortase-mediated transpeptidation. Curr Protoc Protein Sci Chapter 15, Unit 15 3. https://doi.org/10.1002/0471140864.ps1503s56

Poulsen, C., Panjikar, S., Holton, S.J., Wilmanns, M., Song, Y.-H., 2014. WXG100 Protein Superfamily Consists of Three Subfamilies and Exhibits an α-Helical C-Terminal Conserved Residue Pattern. PLOS ONE 9, e89313. https://doi.org/10.1371/journal.pone.0089313

Rathinaswamy, M.K., Fleming, K.D., Dalwadi, U., Pardon, E., Harris, N.J., Yip, C.K., Steyaert, J., Burke, J.E., 2021. HDX-MS-optimized approach to characterize nanobodies as tools for biochemical and structural studies of class IB phosphoinositide 3-kinases. Structure 29, 1371-1381.e6. https://doi.org/10.1016/j.str.2021.07.002

Refai, A., Haoues, M., Othman, H., Barbouche, M.R., Moua, P., Bondon, A., Mouret, L., Srairi-Abid, N., Essafi, M., 2015. Two distinct conformational states of Mycobacterium tuberculosis virulent factor early secreted antigenic target 6 kDa are behind the discrepancy around its biological functions. The FEBS Journal 282, 4114–4129. https://doi.org/10.1111/febs.13408

Renshaw, P.S., Lightbody, K.L., Veverka, V., Muskett, F.W., Kelly, G., Frenkiel, T.A., Gordon, S.V., Hewinson, R.G., Burke, B., Norman, J., Williamson, R.A., Carr, M.D., 2005. Structure and function of the complex formed by the tuberculosis virulence factors CFP-10 and ESAT-6. The EMBO Journal 24, 2491–2498. https://doi.org/10.1038/sj.emboj.7600732

Renshaw, P.S., Panagiotidou, P., Whelan, A., Gordon, S.V., Hewinson, R.G., Williamson, R.A., Carr, M.D., 2002. Conclusive Evidence That the Major T-cell Antigens of theMycobacterium tuberculosis Complex ESAT-6 and CFP-10 Form a Tight, 1:1 Complex and Characterization of the Structural Properties of ESAT-6, CFP-10, and the ESAT-6·CFP-10 Complex: IMPLICATIONS FOR PATHOGENESIS AND VIRULENCE *. Journal of Biological Chemistry 277, 21598–21603. https://doi.org/10.1074/jbc.M201625200

Romagnoli, A., Etna, M.P., Giacomini, E., Pardini, M., Remoli, M.E., Corazzari, M., Falasca, L., Goletti, D., Gafa, V., Simeone, R., Delogu, G., Piacentini, M., Brosch, R., Fimia, G.M., Coccia, E.M., 2012. ESX-1 dependent impairment of autophagic flux by Mycobacterium tuberculosis in human dendritic cells. Autophagy 8, 1357–1370. https://doi.org/10.4161/auto.20881

Sanchez, K.G., Ferrell, M.J., Chirakos, A.E., Nicholson, K.R., Abramovitch, R.B., Champion, M.M., Champion, P.A., 2020. EspM Is a Conserved Transcription Factor That Regulates Gene Expression in Response to the ESX-1 System. mBio 11. https://doi.org/10.1128/mBio.02807-19

Santucci, P., Aylan, B., Botella, L., Bernard, E.M., Bussi, C., Pellegrino, E., Athanasiadi, N., Gutierrez, M.G., 2022. Visualizing Pyrazinamide Action by Live Single-Cell Imaging of Phagosome Acidification and Mycobacterium tuberculosis pH Homeostasis. mBio 13, e00117-22. https://doi.org/10.1128/mbio.00117-22

Schnettger, L., Rodgers, A., Repnik, U., Lai, R.P., Pei, G., Verdoes, M., Wilkinson, R.J., Young, D.B., Gutierrez, M.G., 2017. A Rab20-Dependent Membrane Trafficking Pathway Controls M. tuberculosis Replication by Regulating Phagosome Spaciousness and Integrity. Cell Host & Microbe 21, 619-628.e5. https://doi.org/10.1016/j.chom.2017.04.004

Smith, J., Manoranjan, J., Pan, M., Bohsali, A., Xu, J., Liu, J., McDonald, K.L., Szyk, A., LaRonde-LeBlanc, N., Gao, L.-Y., 2008. Evidence for Pore Formation in Host Cell Membranes by ESX-1-Secreted ESAT-6 and Its Role in Mycobacterium marinum Escape from the Vacuole. Infect Immun 76, 5478–5487. https://doi.org/10.1128/IAI.00614-08

Sørensen, A.L., Nagai, S., Houen, G., Andersen, P., Andersen, A.B., 1995. Purification and characterization of a low-molecular-mass T-cell antigen secreted by Mycobacterium tuberculosis. Infect Immun 63, 1710–1717. https://doi.org/10.1128/iai.63.5.1710-1717.1995

Sreejit, G., Ahmed, A., Parveen, N., Jha, V., Valluri, V.L., Ghosh, S., Mukhopadhyay, S., 2014. The ESAT-6 Protein of Mycobacterium tuberculosis Interacts with Beta-2-Microglobulin (β2M) Affecting Antigen Presentation Function of Macrophage. PLOS Pathogens 10, e1004446. https://doi.org/10.1371/journal.ppat.1004446

Stariha, J.T.B., Hoffmann, R.M., Hamelin, D.J., Burke, J.E., 2021. Probing Protein-Membrane Interactions and Dynamics Using Hydrogen-Deuterium Exchange Mass Spectrometry (HDX-MS). Methods Mol Biol 2263, 465–485. https://doi.org/10.1007/978-1-0716-1197-5_22

Stavri, H., Bucurenci, N., Ulea, I., Costache, A., Popa, L., Popa, M.I., 2012. Use of recombinant purified protein derivative (PPD) antigens as specific skin test for tuberculosis. Indian Journal of Medical Research 136, 799.

Stirling, D.R., Swain-Bowden, M.J., Lucas, A.M., Carpenter, A.E., Cimini, B.A., Goodman, A., 2021. CellProfiler 4: improvements in speed, utility and usability. BMC Bioinformatics 22, 433. https://doi.org/10.1186/s12859-021-04344-9

Tak, U., Dokland, T., Niederweis, M., 2021. Pore-forming Esx proteins mediate toxin secretion by Mycobacterium tuberculosis. Nat Commun 12. https://doi.org/10.1038/s41467-020-20533-1

Vandal, O.H., Pierini, L.M., Schnappinger, D., Nathan, C.F., Ehrt, S., 2008. A membrane protein preserves intrabacterial pH in intraphagosomal Mycobacterium tuberculosis. Nat Med 14, 849–854. https://doi.org/10.1038/nm.1795

Vesosky, B., Rottinghaus, E.K., Stromberg, P., Turner, J., Beamer, G., 2010. CCL5 participates in early protection against Mycobacterium tuberculosis. Journal of Leukocyte Biology 87, 1153–1165. https://doi.org/10.1189/jlb.1109742

Weinstein, J.B., Bates, T.A., Leier, H.C., McBride, S.K., Barklis, E., Tafesse, F.G., 2022. A potent alpaca-derived nanobody that neutralizes SARS-CoV-2 variants. iScience 25, 103960. https://doi.org/10.1016/j.isci.2022.103960

Woolhiser, L., Tamayo, M.H., Wang, B., Gruppo, V., Belisle, J.T., Lenaerts, A.J., Basaraba, R.J., Orme, I.M., 2007. In Vivo Adaptation of the Wayne Model of Latent Tuberculosis. Infection and Immunity 75, 2621–2625. https://doi.org/10.1128/iai.00918-06
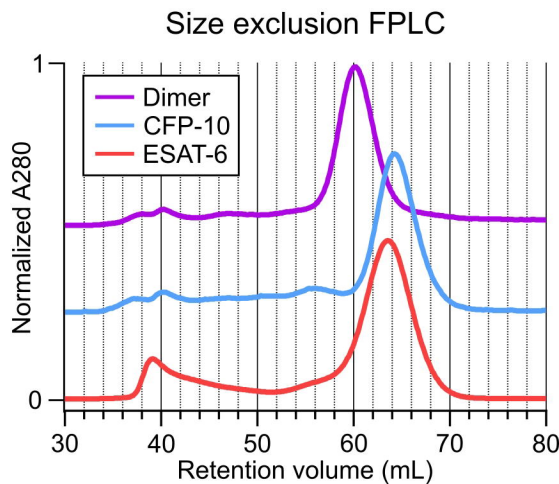
World Health Organization, 2022. Global tuberculosis report 2022. World Health Organization, Geneva.

Xiao, Y., Sha, W., Tian, Z., Chen, Y., Ji, P., Sun, Q., Wang, H., Wang, S., Fang, Y., Wen, H.-L., Zhao, H., Lu, J., Xiao, H., Fan, X., Shen, H., Wang, Y., 2016. Adenylate kinase: a novel antigen for immunodiagnosis and subunit vaccine against tuberculosis. J Mol Med 94, 823–834. https://doi.org/10.1007/s00109-016-1392-5

Yabaji, S.M., Dhamija, E., Mishra, A.K., Srivastava, K.K., 2020. ESAT-6 regulates autophagous response through SOD-2 and as a result induces intracellular survival of Mycobacterium bovis BCG. Biochimica et Biophysica Acta (BBA) - Proteins and Proteomics 1868, 140470. https://doi.org/10.1016/j.bbapap.2020.140470

Yang, C.-S., Lee, J.-S., Lee, H.-M., Sun Shim, T., Woong Son, J., Jung, S.-S., Kim, J.-S., Song, C.-H., Kim, H.-J., Jo, E.-K., 2008. Differential cytokine levels and immunoreactivities against Mycobacterium tuberculosis antigens between tuberculous and malignant effusions. Respiratory Medicine 102, 280–286. https://doi.org/10.1016/j.rmed.2007.08.016

Yang, S., Li, F., Jia, S., Zhang, K., Jiang, W., Shang, Y., Chang, K., Deng, S., Chen, M., 2015. Early secreted antigen ESAT-6 of Mycobacterium Tuberculosis promotes apoptosis of macrophages via targeting the microRNA155-SOCS1 interaction. Cell. Physiol. Biochem. 35, 1276–1288. https://doi.org/10.1159/000373950
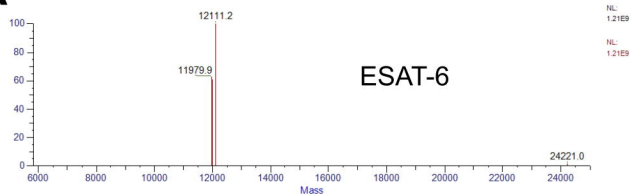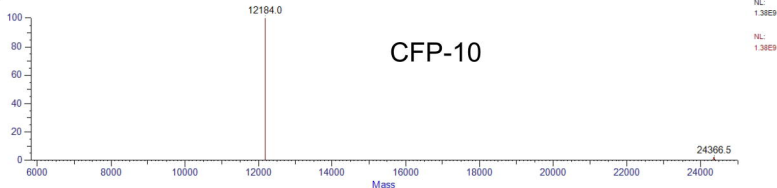
A

ESAT-6

```
         10          20          30          40          50          60
MTEQQWNFAGIEAAASAIQGNVTSIHSLLDEGKQSLTKLAAAWGGSGSEAYQGVQQKWDA
TATELNNALQNLARTISEAGQAMASTEGNVTGMFAELIKLIDTVDLEHHHHHH
```

CFP-10

```
MAEMKTDAATLAQEAGNFERISGDLKTQIDQVESTAGSLQGQWRGAAGTAAQAAVVRFQE
AANKQKQELDEISTNIRQAGVQYSRADEEQQQALSSQMGFKLAALEHHHHHH
```

B

SDS-PAGE   α-His

C

Size exclusion FPLC

A

pMRLB.7 (ESAT-6)

```
            10        20        30        40        50        60
   1 CNNNNNNNCN NNNNNANANT TTGTTTACTT TAAGAAGGAG ATATACAT ATG ACAGAGCAGC
  61 AGTGGAATTT CGCGGGTATC GAGGCCGCGG CAAGCGCAAT CCAGGGAAAT GTCACGTCCA
 121 TTCATTCCCT CCTTGACGAG GGGAAGCAGT CCCTGACCAA GCTCGCAGCG GCCTGGGGCG
 181 GTAGCGGTTC GGAGGCGTAC CAGGGTGTCC AGCAAAAATG GGACGCCACG GCTACCGAGC
 241 TGAACAACGC GCTGCAGAAC CTGGCGCGGA CGATCAGCGA AGCCGGTCAG GCAATGGCTT
 301 CGACCGAAGG CAACGTCACT GGGATGTTCG CAGAGCTCAT CAAGCTTATC GATACCGTCG
 361 ACCTCGAGCA CCACCACCAC CACCACTGA GATCCGGCTGC TAACAAAGCC CGAAAGGAAG
 421 CTGAGTTGGC TGCTGCCACC GCTGAGCAAT AACTAGCATA ACCCCTTGGG GCCTCTAAAC
 481 GGGTCTTGAG GGGTTTTTTG CTGAAAGGAG GAACTATATC CGGATTGGCG AATGGGACGC
 541 GCCCTGTAGC GGCGCATTAA GCGCGGCGGG TGTGGTGGTT ACGCGCAGCG TGACCGCTAC
 601 ACTTGCCAGC GCCCTAGCGC CCGCTCCTTT CGCTTTCTTC CCTTCCTTTC TCGCCACGTT
 661 CGCCGGCTTT CCCCGTCAAG CTCTAAATCG GGGGCTCCCT TTAGGGTTCC GATTTAGTGC
 721 TTTACGGCAC CTCGACCCCA AAAAACTTGA TTANGGTGAT GGTTCACGTA GTGGGCCATC
 781 GCCCTGATAG ACGGTTTTTC GCCCTTTGAC GTTGGAGTCC ACGTTCTTTA ATAGTGGACT
 841 CTTGTTCCAA ACTGGAACAA CACTCAACCC TATCTCGGTC TATTCTTTTG ATTTATNANG
 901 NTTTTGCCGA TTTCGGCCTA TTGGNTAAAA ATGAGCTGAT TTAACAAAAT TTAACGCGAA
 961 TTTANNNAAT ANTAACGCTT ACATTTANNN GCACTTTTCG GGGGAAATGT GCGNGACCCTN
1021 NTTGTTATTT TTCNAANACN TCANTATGNA NCNCTCATGA NANANATANC NTGANAANGNTC
1081 ANAATNTNAA ANNNNNNNNAT NANNATCANA TTTCNNNNCN CCTATNCCNT TTNNNNGNNT
1141 TTNNNTNCNN NTTTNNNN
```

B

pMRLB.46 (CFP-10)

```
            10        20        30        40        50        60
   1 NNNNNNNNNN NNNNNNNNNN NNNNTTTTGT TTAACTTTAA GAAGGAGATA TACATA ATGGC
  61 AGAGATGAAG ACCGATGCCG CTACCCTCGC GCAGGAGGCA GGTAATTTCG AGCGGATCTC
 121 CGGCGACCTG AAAACCCAGA TCGACCAGGT GGAGTCGACG GCAGGTTCGT TGCAGGGCCA
 181 GTGGCGCGGC GCGGCGGGGA CGGCCGCCCA GGCCGCGGTG GTGCGCGCTTC AAGAAGCAGC
 241 CAATAAGCAG AAGCAGGAAC TCGACGAGAT CTCGACGAAT ATTCGTCAGG CCGGCGTCCA
 301 ATACTCGAGG GCCGACGAGG AGCAGCAGCA GAGCGCTGTC CTCGCAAATG GGCTTCAAGCT
 361 TGCGGCCGCA CTCGAGCACC ACCACCACCA CCACTGA GAT CCGGCTGCTA ACAAAGCCCG
 421 AAAGGAAGCT GAGTTGGCTG CTGCCACCGC TGAGCAATAA CTAGCATAAC CCCTTGGGGC
 481 CTCTAAACGG GTCTTGAGGG GTTTTTTGCT GAAAGGAGGA ACTATATCCG GATTGGCGAA
 541 TGGGACGCGC CCTGTAGCGG CGCATTAAGC GCGGCGGGTG TGGTGGTTAC GCGCAGCGTG
 601 ACCGCTACAC TTGCCAGCGC CCTAGCGCCC GCTCCTTTCG CTTTCTTCCC TTCCTTTCTC
 661 GCCACGTTCG CCGGCTTTCC CCGTCAAGCT CTAAATCGGG GGCTCCCTTT AGGGTTCCGA
 721 TTTAGTGCTT TACGGCACCT CGACCCCAAA AAACTTGATT AGGGTGATGG TTCACGTAGT
 781 GGGNCATCGC CCTGATAGAC GGNTTTTCGC CCTTTGACGT TGGAGTCCAC GTTCTTTAAT
 841 AGTGGACTCT TGTTCCAANC TGGAACAACA CTCAACCCTA TCTCGGTCTA TTCTTTTGAT
 901 TTATANGGAT TTTGCCGATT TCGGCCTATT GGTTAAAAAA TGAGCTGANT TAACNAAAAT
 961 TTAACGCGAA TTTTNACNAA ATATTAACGC TTNNAATTTA NNNGGCACTT TTCGGGGAAN
1021 NGNNNNCGGA ACCCCTATTT GGTNNTTTTT TCTAAATACA TNCAANNNGN ANCCGCTCNT
1081 NANANATAAC CNNGANNNNG CTTCANAANN TTGAAAAGGA ANANNNNNAG TATTCNANAN
1141 NTCNNGNNNC CCNNNNNNNN
```
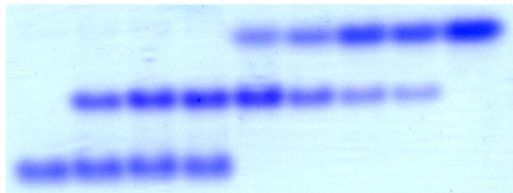
A

ESAT-6

12111.2
11979.9
24221.0

NL:
1.21E9

NL:
1.21E9

B

CFP-10

12184.0
24366.5

NL:
1.38E9

NL:
1.38E9

C

	Computed mass (Da)	Measured mass (Da)	Fractional abundance (%)
ESAT-6	12109.2	12111.2	62
ESAT-6ΔMet1	11978.0	11979.9	38
CFP-10	12313.4	ND	0
CFP-10ΔMet1	12182.2	12184.0	100

A

Native PAGE

ESAT-6:	10	10	10	10	10	7.5	5	2.5	0

μmol

μmol

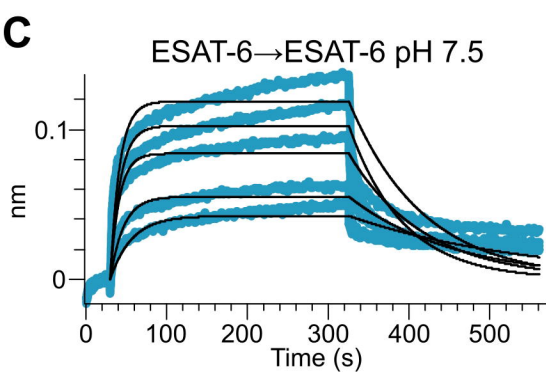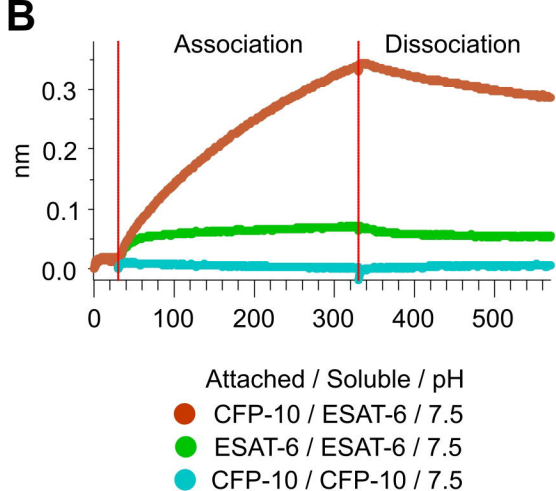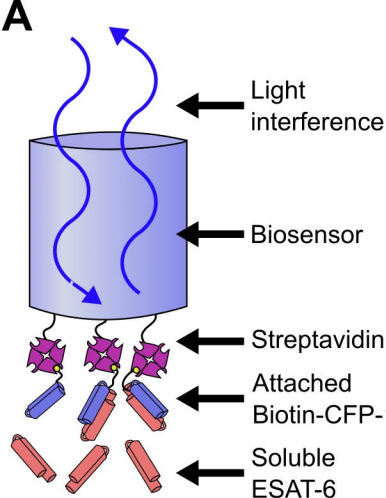| CFP-10:	0	2.5	5	7.5	10	10	10	10	10

B

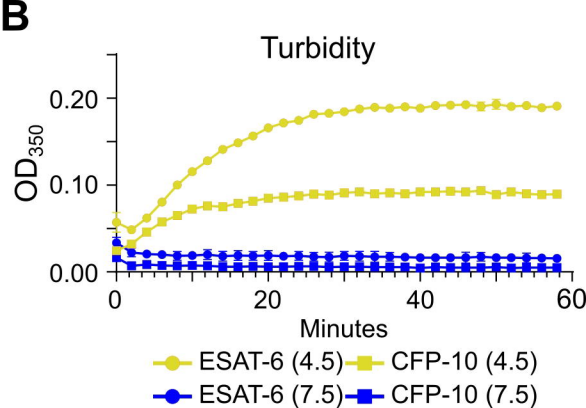## RBC hemolysis
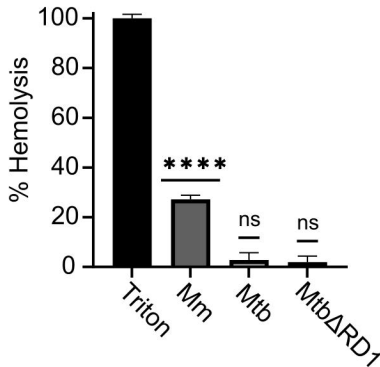
Sheep erythrocyte hemolysis (Purified ESAT-6)

Y-axis: % Hemolysis

X-axis: pH — Triton, 4.5, 5.5, 6.5, 7.5, 8.5

A — Light interference, Biosensor, Streptavidin, Attached Biotin-CFP-10, Soluble ESAT-6

B — Association, Dissociation

Attached / Soluble / pH
- CFP-10 / ESAT-6 / 7.5
- ESAT-6 / ESAT-6 / 7.5
- CFP-10 / CFP-10 / 7.5

C — ESAT-6→ESAT-6 pH 7.5

D — CFP-10→ESAT-6 pH 7.5

E — ESAT-6→ESAT-6 pH 4.5

F — CFP-10→ESAT-6 pH 4.5
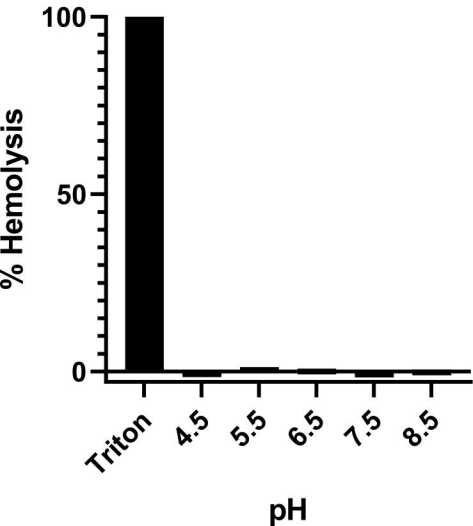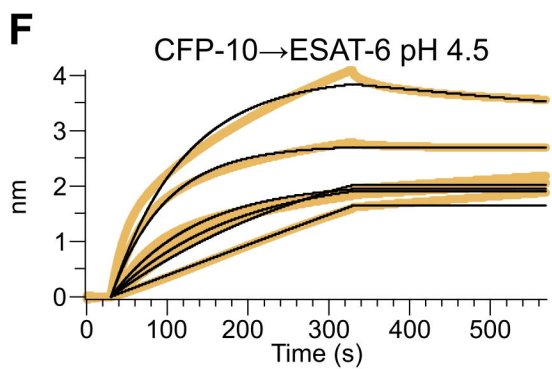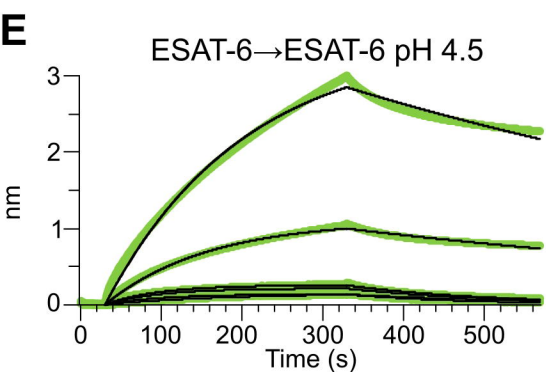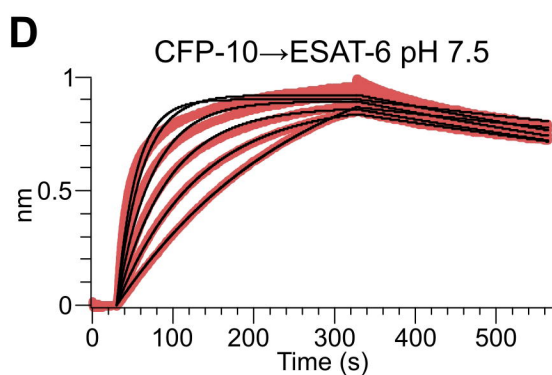
G — Apparent binding constants

Attached	Soluble	pH	K_D (nM)	k_{ON} ($M^{-1}s^{-1}$)	k_{OFF} (s^{-1})
CFP-10	ESAT-6	7.5	0.22	2.8×10^6	6.2×10^{-4}
ESAT-6	ESAT-6	7.5	1.5	5.8×10^6	8.8×10^{-3}
CFP-10	ESAT-6	4.5	0.0004	8.0×10^5	3.9×10^{-7}
ESAT-6	ESAT-6	4.5	3	1.1×10^6	3.3×10^{-3}

H — ESAT-6→ESAT-6

pH 4.5, pH 5.0, pH 5.5, pH 6.0

A

nm
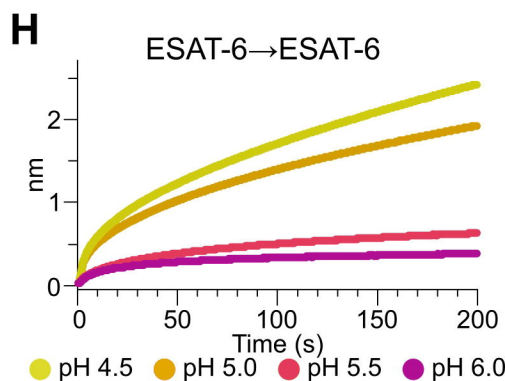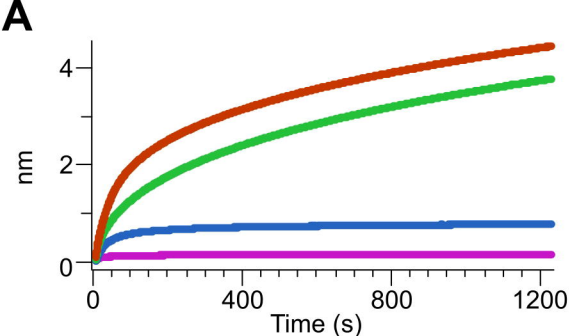
CFP-10→ESAT-6 4.5
ESAT-6→ESAT-6 4.5
CFP-10→ESAT-6 7.5
ESAT6→ESAT-6 7.5

Time (s)

B

Turbidity

OD_{350}

Minutes

ESAT-6 (4.5)   CFP-10 (4.5)
ESAT-6 (7.5)   CFP-10 (7.5)

C

ESAT-6-Lysine-Biotin (~1 biotin incorporated per protein)

MTEQQWNFAGIEAAASAIQGNVTSIHSLLDEGKQSLTKLAAAWGGSGSEAYQGVVQQKWDA
TATELNNALQNLARTISEAGQAMASTEGNVTGMFAELIKLIDTVDLEHHHHHH

ESAT-6-LPETG (before sortase reaction)

MTEQQWNFAGIEAAASAIQGNVTSIHSLLDEGKQSLTKLAAAWGGSGSEAYQGVVQQKWDA
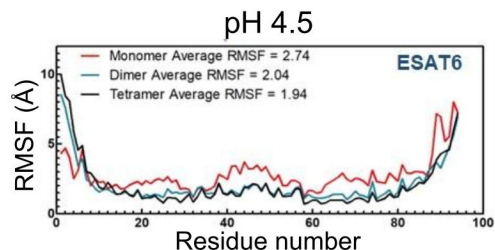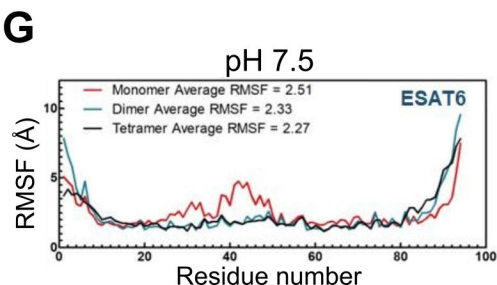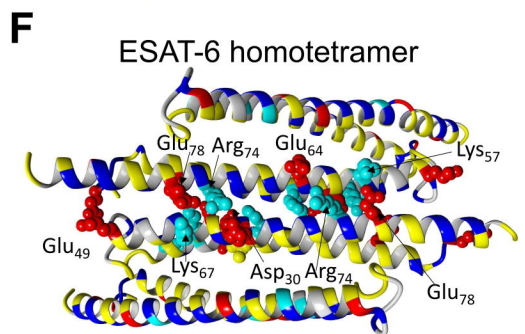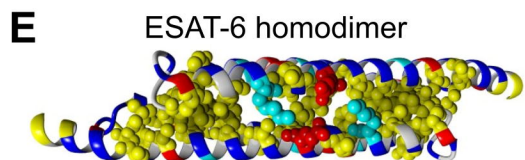TATELNNALQNLARTISEAGQAMASTEGNVTGMFAELPETGGIKLIDTVDLEHHHHHH

D

pH 7.5

normalized nm

Time (s)

E

pH 4.5

normalized nm

Time (s)
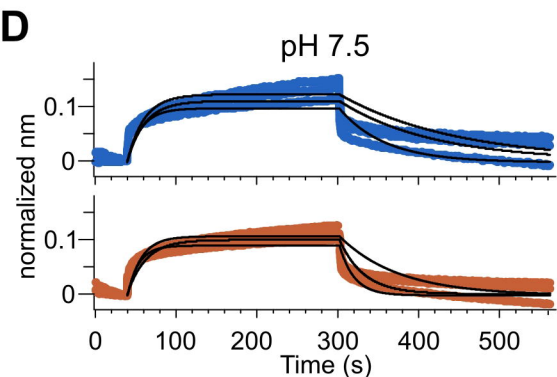
ESAT-6-Lysine-Biotin   ESAT-6-LPETG-Biotin

F
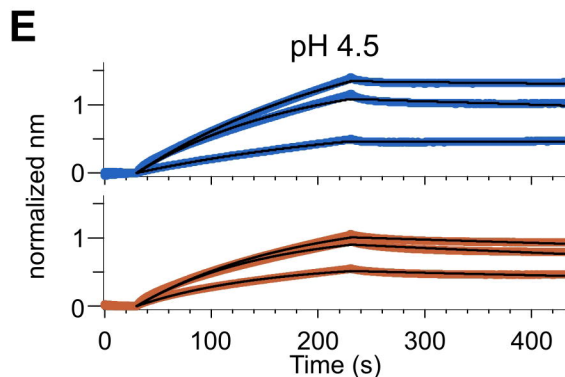
Apparent binding constants

Attached	Soluble	pH	K_D (nM)	k_{ON} ($M^{-1}s^{-1}$)	k_{OFF} (s^{-1})
ESAT-6-LPETG-Biotin	ESAT-6	7.5	12	1.3×10^6	1.6×10^{-2}
ESAT-6-Lysine-Biotin	ESAT-6	7.5	19	1.6×10^6	3.1×10^{-2}
ESAT-6-LPETG-Biotin	ESAT-6	4.5	0.8	2.0×10^5	1.7×10^{-4}
ESAT-6-Lysine-Biotin	ESAT-6	4.5	2.3	2.9×10^5	6.8×10^{-4}

A pH 4.5   pH 7.5   pH 4.5+guanidine

B pH 7.5 — ~21 kDa

C pH 4.5 — ~46 kDa

Molar Mass (black), MALS (red), dRI (blue), UV (green)

D ESAT-6

Glu$_{49}$, Gly$_{47}$, Lys$_{67}$, Glu$_{64}$, Met$_{83}$, Trp$_{43}$, Leu$_{28}$, Ile$_{11}$, C-term

90°

Gly$_{47}$, Glu$_{49}$, Trp$_{43}$, Lys$_{67}$, Glu$_{64}$, C-term

E ESAT-6 homodimer

F ESAT-6 homotetramer

Glu$_{78}$, Arg$_{74}$, Glu$_{64}$, Lys$_{57}$, Glu$_{49}$, Lys$_{67}$, Asp$_{30}$, Arg$_{74}$, Glu$_{78}$

G pH 7.5

Monomer Average RMSF = 2.51
Dimer Average RMSF = 2.33
Tetramer Average RMSF = 2.27
ESAT6

pH 4.5

Monomer Average RMSF = 2.74
Dimer Average RMSF = 2.04
Tetramer Average RMSF = 1.94
ESAT6

A ESAT-6 ELISA

B ESAT-6 / LPETG ESAT-6

C

Attached	Soluble	pH	K_D (nM)	k_{ON} ($M^{-1}s^{-1}$)	k_{OFF} (s^{-1})
E11rv	ESAT-6	7.5	331	5.5×10^4	1.8×10^{-2}
E11rv	ESAT-6 LPETG	7.5	376	1.9×10^4	7.0×10^{-3}

D

E ESAT-6 apo v. ESAT-6 + E11

F ESAT-6

A

	RFP (Total Mtb)	GFP (live Mtb)	Actin	Overlay
E11rv				
Isotype				

B Live/Dead Mtb viability assay

Bacterial burden (GFP/RFP ratio)

****

Isotype   E11rv

C Luminescent Mtb growth assay

Mtb replication (fold change)

- Isotype
- E11rv

0   24   48   72   96   120
hours post infection